Title
ANTIPROTON INTERACTIONS IN HYDROGEN AND CARBON BELOW 200 Mev

Permalink
https://escholarship.org/uc/item/7808533z

Author
Agnew, Lewis E.

Publication Date
1959-07-23

University of California

Ernest O. Lawrence
Radiation Laboratory

Berkeley, California

UCRL-8785 Rev.

cy 2

UNIVERSITY OF CALIFORNIA

Lawrence Radiation Laboratory
Berkeley, California

Contract No. W-7405-eng-48

ANTIPROTON INTERACTIONS IN HYDROGEN AND CARBON BELOW 200 Mev

Lewis E. Agnew, Jr., Tom Elioff, William B. Fowler, Richard L. Lander
Wilson M. Powell, Emilio Segrè, Herbert M. Steiner, Howard S. White
Clyde Wiegand, and Tom Ypsilantis

October 8, 1959

ANTIPROTON INTERACTIONS IN HYDROGEN
AND CARBON BELOW 200 Mev

Lewis E. Agnew, Jr., Tom Elioff, William B. Fowler, Richard L. Lander
Wilson M. Powell, Emilio Segrè, Herbert M. Steiner, Howard S. White
Clyde Wiegand and Tom Ypsilantis

Lawrence Radiation Laboratory
University of California
Berkeley, California

October 8, 1959

ABSTRACT

About 500 antiprotons in a partially purified antiproton beam have been observed to enter the 30-in. propane bubble chamber. An arrangement of counters identified the antiproton events, thus reducing scanning to a minimum and also providing a sample of antiprotons free of scanning bias. The antiprotons entered the propane at a kinetic energy of 220 Mev and were brought to rest. Scattering and annihilation interactions in both hydrogen and carbon have been observed as a function of antiproton energy. Differential scattering cross sections have been obtained, and the following total cross sections have been measured for antiproton kinetic energies, T, in the ranges 75 to 137.5 Mev and 137.5 to 200 Mev:

Interaction	Cross section, σ (mb)	
	$75 \leqslant T \leqslant 137.5$	$137.5 \leqslant T \leqslant 200$
($\bar{p}$-p) elastic	66 ± 17	56 ± 14
($\bar{p}$-p) annihilation	112 ± 23	60 ± 18
($\bar{p}$-C) elastic (5 deg (lab) cutoff)	345 ± 60	255 ± 45
($\bar{p}$-C) annihilation	474 ± 76	360 ± 65

The above results show satisfactory agreement with the Ball-Chew theory where comparison can be made.

The details of the annihilation process in hydrogen and carbon have been observed. One feature of the experiment is that, in contrast to previous studies of annihilation products, we are able to make a direct observation of the neutral pions through pair production by π^0 decay photons. The significant results for carbon and hydrogen annihilations at an average antiproton kinetic energy $\tilde{=}$ 100 Mev are:

	Hydrogen annihilations		Carbon annihilations	
Annihilation product	Multiplicity	Average total energy (Mev)	Multiplicity	Average total energy (Mev)
π^-	1.53 ± 0.08	402 ± 21	1.58 ± 0.07	366 ± 13
π^+	1.53 ± 0.08	379 ± 19	1.33 ± 0.08	371 ± 13
π^0	1.60 ± 0.50	356 ± 110	1.15 ± 0.30	342 ± 90

In addition to the above-listed annihilation products, the carbon stars contained nucleons that carried off more than 188 Mev per star. When pion absorption is considered, the carbon result of 4.1 ± 0.3 pions per annihilation is consistent with the observed hydrogen multiplicity of $4.7 \pm .0.5$ pions. Pion energy spectra and frequency distributions, as well as other details, have been obtained.

Seventeen strange particles have been identified among the products of all the annihilations. This indicates that the production of a pair of K mesons occurs in $4.0 \pm 1.0\%$ of all annihilations. The average total energy per K pair is greater than 1200 Mev.

The charge-exchange process $\bar{p} + p \to \bar{n} + \bar{n}$ has been observed and, based on six possible events, we obtain the result $\lambda \gtrsim 630 \text{ g/cm}^2$ for the mean free path in propane $(50 \leq T_{\bar{p}} \leq 150 \text{ Mev})$.

ANTIPROTON INTERACTIONS IN HYDROGEN
AND CARBON BELOW 200 Mev*

Lewis E. Agnew, Jr.,[†] Tom Elioff, William B. Fowler,[§] Richard L. Lander,
Wilson M. Powell, Emilio Segrè, Herbert M. Steiner, Howard S. White,
Clyde Wiegand, and Tom Ypsilantis

Lawrence Radiation Laboratory
University of California
Berkeley, California

October 8, 1959

I. INTRODUCTION

Since the discovery of the antiproton by Chamberlain, Segrè, Wiegand,
and Ypsilantis in 1955,[1] several counter and emulsion experiments have been
performed in order to determine the interaction characteristics of the antiproton,
$\bar{p}$.[2-9] In addition, an experiment was recently performed with the hydrogen
bubble chamber.[10] A thorough review of the experimental and theoretical
developments on antinucleons has been given recently by Segrè.[11]

Among the interesting properties of the antiproton that have been observed
are these.

(a) Cross sections for scattering and annihilation are large.

(b) Antiproton-nucleon annihilations near rest give about multiplicity of
about five pions.

(c) The production of K mesons in antiproton-nucleon annihilation is
observed rarely.

(d) Little is known of the charge-exchange process $(\bar{p} + p \rightarrow \bar{n} + n)$ by
which the antineutron was detected electronically.

The 30-inch propane bubble chamber is well suited to the observation
of the above phenomena. For instance, antiproton cross sections become

difficult to measure by counter techniques at low energies, whereas nuclear emulsions are undesirable because they consist of a variety of complex nuclei. The propane bubble chamber, on the other hand, allows observation of the very fundamental $\bar{p}$-p processes. An understanding of the low-energy (i.e. ~100 Mev) $\bar{p}$-p interaction is essential to any complete theory of nuclear forces. One theory has been proposed by Ball and Chew[12] which retains the structure of the nucleon-nucleon interaction suggested by Gartenhaus[13] and by Signell and Marshak,[14] with reasonable modifications to fit the nucleon-antinucleon case. Our results support the Ball-Chew theory on $\bar{p}$-p scattering and annihilation, within the validity of our statistics. It should be pointed out that a recent counter experiment[9] and accumulated emulsion results[15] also support the theory.

The annihilation process may be especially well observed in a bubble chamber. Not only may the charge of the annihilation products be determined, but momentum is also easily obtained. Furthermore, the large propane chamber permits the direct observation of π^0 annihilation products through pair production by the π^0-decay photons. Our results of 4.7±0.5 pions per star is to be compared to the 5.36±0.3 obtained in Berkeley[8] and 4.92±0.13 obtained in Rome[16] with emulsion, and to 4.94±0.31 obtained with the hydrogen bubble chamber.[10] For both the emulsion and the hydrogen bubble chamber, π^0 production is estimated through charge-independence arguments and energy considerations.

The natural attempt to explain the pion multiplicity by means of the Fermi statistical model has not been successful. Such high multiplicities as are observed seem to require a volume-of-interaction parameter Ω about 10 times the value expected when the Compton wave length of the pion is used as a radius. A different approach by Koba and Takeda,[17] wherein the pion cloud and nucleon core are treated separately, succeeds in predicting the high multiplicity observed.

We have been able to establish the rate at which antiproton annihilations produce K- meson pairs. While observation of charged K mesons is often difficult, we have a high efficiency for detecting short-lived neutral strange particles. Our finding that only $4.0 \pm 1.0\%$ of all annihilations yield a pair of K mesons is in disagreement with the various forms of the Fermi statistical model, which predict a higher ratio of K to π production.

The charge-exchange process, $\bar{p} + p \rightarrow \bar{n} + n$, heretofore observed only electronically, [6,18] is especially adapted to bubble chamber observation. However, charge exchange seems to be relatively infrequent compared with annihilation and elastic scattering, and the scope of our experiment permits little more than confirmation of the process.

II. APPARATUS AND METHOD
A. The Antiproton Beam

The antiproton beam and its partial purification have been described briefly elsewhere.[19] Figure 1 is a diagram of the apparatus. Table I gives descriptions of components of the apparatus. The 30-inch propane bubble chamber is described elsewhere.[20]

The 6.1-Bev circulating proton beam of the Berkeley Bevatron is directed upon a 6-in.-long beryllium target (T in Fig. 1). Negative particles produced at the target are deflected outward by the Bevatron's magnetic field and magnet M_1 so that only those of 970 Mev/c momentum can be delivered to a beryllium absorber at A_1. Upon leaving A_1, the antiprotons have 848 Mev/c, while pions have 905 Mev/c. Deflection of the beam at M_2 causes a separation at A_2 based on the momentum difference between the two kinds of particles. This process of separation by differential absorption is then repeated, by using the counters plus 9.4 g/cm^2 of beryllium as absorber at A_2 for the deflection at M_3. The antiproton beam has a momentum of 729 Mev/c upon leaving A_2, but only 684 Mev/c after passing through the chamber window and entering the propane. The three quadrupole focusing magnets serve to maintain high beam intensity over the long channel. Except for the addition of a second separation, the beam is quite similar to that described in a previous paper.[8]

About 33 particles per 10^{10} protons hitting the target arrive at the center of the bubble chamber. The contaminating particles at the bubble chamber are mostly muons which can still enter the bubble chamber, but they are displaced to one side.

Table I

Components of the apparatus	
Symbol	Description
T	Bevatron target for production of antiprotons (beryllium, 0.5X0.5X6 in.)
M_1, M_2, M_3	Deflecting magnets: 15-, 40-, and 26-deg bending, respectively.
Q_1, Q_2, Q_3	Quadrupole focusing magnets of 8-in. aperture.
M_4	Deflecting magnet used in emulsion exposures.
E	Emulsion stack.
BC	Propane bubble chamber: 30 in. along the beam direction, 20 in. transverse to the beam, 6.5 in. deep, and filled with propane of density 0.42 g/cm^2.
A_1	Beryllium absorber: 32 g/cm^2 (for bubble chamber beam).
A_2	Absorber equivalent to 25 g/cm^2 of beryllium (for bubble chamber beam).
S_1	Plastic scintillation counter: 3.5X3.5 in. by 0.5 in. thick.
C_1	Čerenkov counter, H_2O radiator, 4X4X2 in. thick.
F_1	Fitch-type Čerenkov counter: CS_2 radiator 4 in. in diam by 2.25 in. thick.
S_2	Plastic scintillation counter: 7.25X2.5X0.25 in. thick.
Pb	Lead collimators.

The ratio of $\bar{p}$'s to undesired particles after the bubble chamber window is 67×10^{-6}. At the same momentum, the ratio of antiprotons to undesired particles at the target is about 1.6×10^{-6}. The purification factor is thus 42. For the entire experiment, the beam averaged about two antiprotons observed per hour of operation. Normal Bevatron beam level was 2×10^{10} protons per pulse at 600 pulses per hour.

B. Proton Calibration

By making minor changes in the operation of the apparatus, it was possible to extract a positive-proton beam. The protons were scattered from a copper target properly located in the Bevatron. The magnetic fields of all magnets were reversed to allow the transmission of positively charged beam, but the field magnitudes and all absorbers were kept identical to those used for antiprotons. The double momentum analysis (in M_2 and M_3) guaranteed the momenta to be the same within 2%. The proton beam was used to "calibrate" the chamber for antiprotons and to check the system of triggering counters.

The ranges of more than 1000 protons entering the chamber were measured, and the distribution is shown in Fig. 2. It is seen that the incoming protons may be divided into two groups, a homogeneous group giving rise to a sharp peak and a smaller group having a continuous energy distribution downward from the maximum. Protons contributing to the sharp peak entered the bubble chamber window with a momentum of 684 ± 20 Mev/c as determined by their range of 54 ± 5 cm. The short-range protons are due primarily to variations in wall thickness in the immediate vicinity of the window.

Besides confirming the beam energy, studies of the position, ionization, and curvature of the stopping protons helped set up reliable criteria for antiproton identification.

C. Electronic Selection of Antiprotons

It was recognized in the planning stage of the experiment that the rate

of appearance of antiprotons in the bubble chamber would be a few per hour. This

posed a serious scanning problem, for there are 600 Bevatron beam pulses per

hour. Not only would finding the antiprotons be a tedious job, but also it seemed

evident that scanning might be biased toward those events that were most easily

discovered by virtue of a many-pronged annihilation. These two difficulties were

in great measure avoided through the use of a system of counters which selected

those beam pulses for which the probability of an antiproton was high. In typical

operation, the bubble chamber expansion is initiated with each Bevatron pulse

about 45 msec before the beam arrives, and the lights are flashed some 6 msec

after a 2-msec beam pulse passes through. This delay of the lights, which is

necessary for proper bubble growth, is sufficient to allow the lights to flash only

upon a command from the counters.

The counters are shown in Fig. 1 and briefly described in Table I. The

two scintillation counters S_1 and S_2 are spaced 25 ft apart and define a time-

of-flight measurement. The Fitch-type Čerenkov counter, F_1 , responds to

particles of velocity corresponding to $0.62 \lesssim \beta \lesssim 0.78$. The water Čerenkov

counter, C_1 , responds only to particles with $\beta > 0.75$. At F_1 , antiprotons in

the beam have $\beta = 0.67$, while the mesons approach $\beta = 1$. The requirements

for an antiproton to be detected are that (a) there is a proper time delay be-

tween signals from S_1 and S_2; (b) a signal appears from F_1; and (c) no

signal appears from C_1 .

Bubble chamber pictures were taken upon receipt of a signal triggered by

proper coincidence of signals from S_1 , S_2 , and F_1 . So that all antiproton

events would be photographed, the sensitivity of the trigger was adjusted so that

more pictures were taken than just those that contained antiprotons. Signals

from all four counters were displayed on an oscilloscope and photographed on

35-mm film. A simple numbering device suitably cross-indexed the oscilloscope

traces and the bubble chamber film. Upon scanning the oscilloscope film it was

possible to select about 4% of the bubble chamber pictures as possibly containing

antiprotons. In half of these cases, unhurried scanning yielded an antiproton event.

D. Scanning and Measuring

A complete double scan was made of all bubble chamber pictures that were electronically predicted to contain an antiproton. Only physicists participated in the scanning.

Each picture electronically selected was scanned with only the first 20 cm (about 1/3 of the antiproton range) visible. This was accomplished by means of a simple mechanical shutter attached to a projection scanning table. An attempt was made to identify the antiprotons by their ionization of approximately twice minimum. This was a fairly successful method: some 65% of the antiprotons were identified in the first 20 cm of track by ionization alone. Half of the remainder were not identified by track alone because they made spectacular interactions within the first 20 cm. Others were not identified in the first 20 cm of track because of overlapping μ-meson tracks or occasional poor illumination near the chamber entrance.

Electronic selection, by reducing the number of pictures, permits almost unlimited scanning time per picture. Those antiprotons that were not recognized in the first 1/3 of their range were found upon thorough search of the entire chamber. Final identification usually amounted to no more than a careful check of ionization near mid-chamber, where a value of ~4 times minimum is expected.

Upon locating an antiproton interaction, each scanner made bubble-count ionization estimates, as well as tentative identification, for every prong. Each scanner also gave his interpretation of the event and specified detailed measuring procedures. Upon completion of measurement, both scan reports were compared with each other and with the measured momentum for each track segment. Any serious discrepancy between particle momentum and observed ionization was resolved by rescanning and remeasuring.

All events were measured by tracing out each track on the 70-mm film
(in both views) with a digitized microscope that punches track coordinates directly
into IBM-650 data cards.   An IBM program was then used to make a least-squares
fit to a parabola projected on the horizontal plane and a straight line in the vertical
plane.   The slope of the straight line and the chord-sagitta relationship of the curve
are sufficient to specify momentum upon further IBM computing, once magnetic-
field values within the chamber are known.

Routine computations give the dip and azimuthal angles of each track
measured in addition to the momentum.   Errors are assigned to each measured
quantity as a part of the program.   Errors reflect not only the internal consistency
of the measured points along each track, but also known physical effects.   For
example, multiple scattering puts an accuracy limit of $\pm 10\%$ on momentum
measurements by track curvature even for energetic particles, while momenta
determined by range are much more accurate.   Typical errors on angular
measurements vary from a few tenths of a degree to a few degrees.   Absolute
positions within the chamber can be measured within a few millimeters, while
relative positions can be determined much more precisely.

III. RESULTS: ANTIPROTON CROSS SECTIONS
A. Antiproton Path Length and Kinetic Energy

At the conclusion of the scanning and measuring processes, the total antiproton path length in the propane was computed. All 471-identified antiprotons upon which complete measurements could be made were accepted, while 84 events which were not measurable because of imperfect film were excluded. The actual determination of path length for each individual event is easily done; however, it is a little more difficult to assign an energy to a specific point along the track. Annihilations in flight restrict the use of residual range, and curvature measurements on low-energy antiprotons become inaccurate because of multiple scattering. A positive proton beam that was passed through the same momentum-analysis apparatus (see Section II B) was used to "calibrate" the beam, and the antiprotons were assumed to have the same energy distribution as the protons upon leaving the final counter S2. Large variations in wall thickness at the window of the chamber cause a significant number (20%) of "short-range" protons.

Each antiproton was assigned a kinetic energy at its first major interaction, on the basis of the peak of the proton range distribution in the chamber, unless it was deemed to be a "short-range" $\bar{p}$. These short-range $\bar{p}$'s were detected by requiring (a) the ionization to be heavy, (b) the position of the particle to indicate that it came through wall rather than window, and (c) the curvature to indicate that the $\bar{p}$ was slower than the main groups of antiprotons.

The path lengths are summarized in Table II.

Table II

Summary of $\bar{p}$ path lengths

$\bar{p}$ kinetic energy (Mev)	50 to 75	75 to 100	100 to 125	125 to 150	150 to 175	175 to 200
$\bar{p}$ path length (cm)	1424	2194	2534	2996	3653	3108
H (g/cm^2)	107	166	191	226	276	234
C (g/cm^2)	483	745	860	1017	1240	1055

B. Antiproton-Proton Elastic Scattering

A preliminary report on $\bar{p}$-p elastic scattering has already been published.[19] We now present somewhat different results after thoroughly scanning and measuring all events. The following corrections to the earlier work were significant: (a) the path length was measured accurately (it is now 3% shorter), (b) four antiprotons that scattered elastically and left the chamber before annihilating were discovered, and (c) the cutoff-angle criterion was improved.

In establishing a cutoff angle we have adopted the criterion that the recoil proton must have a range of at least 1 mm, which is sufficient to distinguish a $\bar{p}$-p scattering from a $\bar{p}$-C scattering. A cutoff angle determined in this way is dependent upon antiproton energy. For the energy interval 75 to 137.5 Mev, a center-of-mass (c.m.) angle of 25 deg is an appropriate cutoff, while 20 deg (c.m.) is suitable for the interval 137.5 to 200 Mev.

The 471 antiprotons that contributed to our path length had 42 observed $\bar{p}$-p elastic scatterings, including 11 with scattering angle less than θ_c. Each event was measured and verified by use of the unique two-body kinematics. In calculating cross sections we have divided the data into the two energy intervals indicated in the preceding paragraph. Table III gives the results, of which the average is 62 ± 12 mb (good geometry) over the entire range from 75 to 200 Mev.

The optical-theorem relationship $\frac{d\sigma}{d\Omega}$ (0 deg) $\geq (\frac{\sigma_t k}{4\pi})^2$ was used to make the correction to good geometry. The total cross section σ_t used to obtain $\frac{d\sigma}{d\Omega}$ (0 deg) was estimated by using the total elastic cross section up to the cutoff and the annihilation cross section presented in Table IV. We assumed that $\frac{d\sigma}{d\Omega}$ was constant from $0°$ to θ_c (to compensate for the missing $\left[\text{Re } f (0 \text{ deg}) \right]^2$) and corrected the cross section by integrating from 0 deg to θ_c.

Table III

$\bar{p}$-p Elastic scattering[a]		
$\bar{p}$ kinetic energy interval (Mev)	$75 \leqslant T_{\bar{p}} \leqslant 137.5$	$137.5 \leqslant T_{\bar{p}} \leqslant 200$
$\bar{p}$-p cutoff angle θ_c (c.m.) (deg)	25	20
$\sigma_{el}(\theta_c)$ (mb)	50 ± 13	46 ± 11
σ_{el} (0deg) (mb)	66 ± 17	56 ± 14

[a]A large cutoff angle is adopted to safeguard against confusion with elastic scatterings off carbon nuclei. The correction to σ_{el} (0 deg) is explained in the text.

Table IV

Annihilation cross sections for antiprotons in hydrogen and carbon. Results are averaged over the energy ranges indicated.		
Antiproton kinetic energy, T (in Mev)	$75 \leqslant T \leqslant 137.5$	$137.5 \leqslant T \leqslant 200$
$\bar{p}$-p annihilation cross section (mb)	112 ± 23	60 ± 18
$\bar{p}$-C annihilation cross section (mb)	474 ± 76	360 ± 65

This correction, which amounts to almost 25% of the good-geometry result, agrees satisfactorily with that predicted by the theoretical angular distribution according to Fulco,[21] who used the Ball-Chew model.[12]

The Ball-Chew theory of the nucleon-antinucleon interaction, which is apparently successful, is based on the Yukawa interaction, with the addition of a spin-orbit term and an absorbing central core that accounts for annihilation. The theory has been applied only to moderate energies. The original calculations were made at 140 Mev, at which precise knowledge of the core radius is not crucial. At higher energies the details of the annihilation boundary condition become important. Below 50 Mev the WKB method of calculation breaks down. Ball and Fulco have extended the original calculations from 50 to 260 Mev.[22] Figure 3 compares their predictions with our results for $\bar{p}$-p reactions.

In Fig. 4 we present the angular distribution of the $\bar{p}$-p elastic scattering. Because of the small number of events (only 31 with scattering angle greater than θ_c = 25 deg), we have plotted one distribution for all antiproton energies from 75 to 200 Mev. The theoretical differential scattering cross section at 140 Mev given by Fulco[21] is also shown for comparison.

A summary of all $\bar{p}$-p elastic scatters reported to date in nuclear emulsions has been collected by G. Goldhaber[23] and is presented in Table V. Our results are in the same energy region and are included for comparison. By grouping together all the data from emulsions and the propane bubble chamber, we obtain an average value of σ_{el} = 60 ± 8 mb at an average energy of about 137 Mev. This result is in good agreement with the Ball-Chew prediction of 73 mb at 140 Mev.

Table V

Summary of all $\bar{p}$-p data reported to date, excluding counter data

	Energy interval (Mev)	Path length (g/cm^2 of H)	Average energy (Mev)	σ_{el} ($\bar{p}$-p) (mb)
1. Emulsions	75 to 200	1006	140	58 ± 10
2. Propane chamber	75 to 200	1093	135	62 ± 12
3. 1 and 2 combined		2099	137	60 ± 8
4. Ball-Chew theory			140	73

C. Antiproton-Carbon Elastic Scattering

Although an earlier report has been made,[24] we present here a final analysis of p̄-C elastic scattering. As mentioned before, scanning becomes very inefficient at small angles. For this reason we have established an angle of 3 deg projected upon the horizontal plane as a scanning limitation, thus we ignore those observed events with a smaller projected angle. A correction based on camera separation and height above the chamber, and on an assumed uniform distribution in azimuth of the p̄-C scatterings, is then applied to compensate for the missing events. This correction factor varies from 1.6 at a laboratory-system angle of 5 deg to 1.1 at 20 deg (lab). Another correction, which is only 3%, is needed to remove p̄-p elastic scatterings that leave no recoil proton and hence are indistinguishable from p̄-C elastic scatterings.

We have adopted a cutoff angle of 5 deg (lab) for all p̄-C elastic scattering events. This essentially eliminates the consideration of Coulomb effects. An uncorrected total of 91 scatterings of more than 5 deg was obtained in the antiproton energy region from 200 Mev to rest.

For the purpose of calculating elastic cross sections on carbon, we placed most of the events into two groups: antiproton kinetic energies from 75 to 137.5 Mev, and from 137.5 to 200 Mev. Our results for θ (lab) $\geqslant$5 deg are shown in Fig. 5. Also shown in Fig. 5 are the theoretical predictions of an optical-model calculation by Bjorklund and Fernbach using the nucleon-antinucleon phase shifts of Ball and Chew and the method of Riesenfeld and Watson to obtain the well-depth parameters.[22,25] This theory also predicts differential scattering cross sections for which calculations have been made at several energies. Our limited number of events does not warrant the presentation of more than one angular distribution including all events from 75 to 200 Mev, which is shown in Fig. 6. The theoretical differential cross section at 140 Mev is included for comparison.[25]

D. Annihilation Cross Sections

Of the 471 antiprotons that contributed to our path length only 448 had tracks that terminated in the chamber; the rest scattered out at the top or bottom. Each annihilation was classified as having occurred in a carbon or hydrogen nucleus. Annihilations that result in an imbalance of charge or have nucleons among the products are obviously carbon stars. A hydrogen annihilation must have only pions (or K mesons) as products, and the net charge must be zero. All annihilations that fitted these conditions were classified as hydrogen stars, although the conditions were not sufficient to fix the assignment. It is clear that an anti-proton may annihilate within a carbon nucleus in such a way as to be indistinguish-able from a hydrogen annihilation (e.g., in such a way as to "fake" a hydrogen annihilation), and a correction must be made for this effect before annihilation cross sections are calculated.

Of our 448 terminating antiproton tracks, we were able to designate 302 annihilations as definitely carbon, and 146 as possibly hydrogen. Only 127 of the carbon annihilations were caused by antiprotons with more than 50-Mev kinetic energy, but 90 of the possibly hydrogen stars occurred in this manner.

In order to determine the annihilation cross sections, we must make corrections in the assignment of in-flight annihilations to hydrogen and carbon, i.e., corrections must be made for the "fake" $\bar{p}$-H stars, and also for antiproton charge exchange that simulates $\bar{p}$-H annihilation into neutral pions.

The correction to account for fake $\bar{p}$-H annihilation is determined by comparing the fake $\bar{p}$-H annihilation to a direct counterpart, the fake $\bar{p}$-n star, assuming they are equally probable. This is justified as follows.

The antiproton must annihilate on either a neutron or a proton within the carbon nucleus. The annihilation cross sections for $\bar{p}$-p and $\bar{p}$-n reactions are predicted to be the same,[12] and there is experimental evidence that they

are equal at a higher energy.[5] Since the carbon nucleus contains equal numbers

of protons and neutrons, it seems likely that within the carbon nucleus equal numbers

of $\bar{p}$-p and $\bar{p}$-n annihilations take place.

If the pions emerge without interacting inside the carbon nucleus, then

our assumption of equally probable fake $\bar{p}$-p and $\bar{p}$-n stars is justified. Moreover,

if a pion does interact before leaving the carbon nucleus, ejecting a proton, the

resulting star can not be confused with a hydrogen star. For such pion inter-

actions, it is possible to show by I-spin arguments that the fake $\bar{p}$-p and $\bar{p}$-n

annihilations are still almost equally probable.

Of the 40 annihilations that satisfied the conditions of a $\bar{p}$-n star, 15

occurred at $\bar{p}$ energies of more than 50 Mev. This means that we should expect

that 15 of the in-flight hydrogen annihilations are really carbon, or in other words

that 83% of the "possibly hydrogen" are indeed $\bar{p}$-H annihilations.

Table IV gives the annihilation cross sections on carbon and hydrogen

after corrections. Average results are presented for two equal energy intervals

from 75 Mev to 200 Mev, and are based on 54 hydrogen stars and 100 carbon stars.

Statistical errors on both the "raw" numbers and the corrections have been

combined to yield the errors stated. These results agree qualitatively with the

large absorption cross sections observed previously at various antiproton

energies.[4,5,8,9] The Ball-Chew model predicts $\bar{p}$-p annihilation cross sections

of 110 mb at 50 Mev and 74 mb at 140 Mev.[22] Predictions of this model are

compared with our experimental results in Fig. 3. Although annihilation in

the Ball-Chew model is not strongly dependent on core size, it is dependent in

a cruder model suggested by Koba and Takeda.[17] There annihilation occurs upon

an incoming antiproton of wave length λ (c. m.) hitting an absorbing core of

radius a to give $\sigma_{ann} = \pi (a + \lambda)^2$. For this model our results would suggest

$a \simeq 0.6 \, \hbar/m_\pi c$.

IV. RESULTS: MISCELLANEOUS

A. Antiproton Charge Exchange and the ρ Stars

The antiproton charge-exchange reaction $\bar{p} + p \to \bar{n} + n$ was used in demonstrating the antineutron.[18,6] This was a counter experiment. A bubble chamber offers the possibility of visual observation of both the charge-exchange process (disappearance of a $\bar{p}$) and the subsequent $\bar{n}$ annihilation (a neutral-produced star of large energy). Such an event has been observed in this experiment, and has been reported earlier.[19]

Unless antineutron annihilation occurs within the chamber, the charge-exchange process is difficult to distinguish from a $\overline{p}$-p annihilation in which all final-state pions are neutral (a "ρ star"). We have found eleven cases in which the antiproton track ends within the chamber with no star. Three of these cases have verified photon pair conversions and thus must be considered ρ stars.[26] Two others occur at the end of the antiproton range and are also considered ρ stars, on the premise that charge exchange at very low energy will almost certainly lead to an $\bar{n}$ annihilation within the chamber. We are left with the following situation:

	Charge exchange	ρ stars	Undetermined
Number of events	1	5	5

The undetermined events may be assigned as either charge exchanges of ρ stars. In order to make the assignment, we assume that the ρ star produces an average of at least 3.5 neutral pions and then calculate the probability, P, of identifying the event through pair production by a gamma ray from a π^{o} decay. This probability is $P \geqslant 0.4$. Furthermore, we estimate upon assuming charge-exchange scattering to be isotropic and the $\bar{n}$ annihilation cross section to be the same as that of the $\bar{p}$, that the probability of detecting an antiproton charge

exchange by observing the $\bar{n}$ star within the chamber is about 0.3. These est-
imates enable us to assign two of the five undetermined events as charge ex-
changes, and three as p stars, to get the following:

	Charge exchange	p star
Observed events	1	5
Assigned events	2	3
Total	3	8

No really precise measurement of antiproton charge-exchange cross
section has yet been made for low antiproton energies. The only previous re-
port for energies below 200 Mev gives $\sigma_{(\bar{p} + p \to \bar{n} + n)} = 10^{+2}_{-3}$ mb at 133 ± 13
Mev in a counter experiment.[9] Unfortunately, our bubble chamber experiment
permits little more than confirmation of the existence of the process. Because
we are confident of our ability to identify antiprotons, especially at kinetic energies
below 150 Mev, we are able to set an upper limit (with poor statistics) on the
charge-exchange process. For the purposes of an upper limit, we use the
maximum of the possible charge-exchange events, namely six, rather than the
estimated result of three events. For the mean free path for charge exchange
in propane in the energy interval 50 to 150 Mev, we obtain $\lambda \gtrsim 630$ g/cm^2.
This is consistent with charge-exchange cross-section limits $\sigma \lesssim 15$ mb for
hydrogen (assuming all six events occurred on hydrogen), and $\sigma \lesssim 39$ mb
for carbon (assuming all six events occurred on carbon).[27]

The Ball-Chew model predicts $\sigma_{(\bar{p} + p \to \bar{n} + n)}$ to be 31 mb at 50 Mev
and 21 mb at 140 Mev.[22]

B. Antiproton Interactions below 75 Mev

Upon coming to rest, an antiproton must be captured by either carbon or
hydrogen, although the proportion captured by each is uncertain.[28] Antiproton
capture by hydrogen produces the neutral system protonium, with an estimated

principal quantum number of about n = 30. This estimate of the principal

quantum number is based on the assumption that protonium is formed with a

radius approximately that of the hydrogen atom because at larger distances, the

charge of the proton is probably screened by an electron. The arguments that

follow are all based on n = 30 for protonium, but the conclusions remain un-

changed down to n = 15.

Protonium with n = 30 is a relatively stable system against radiative

transition. Its transition probability (T.P.), if we consider all possible final

states and assume that , in the initial state, the substates of the orbital quantum

numbers l are occupied according to their statistical weights, is T.P.

~ 1×10^7 sec^{-1}. Even so, radiative transition is more probable than annihilation,

as has been pointed out by Bethe and Hamilton,[29] except for S states, in which

annihilation can occur. For n = 30, the weight of the S state (again assuming

population of the substates of l according to their statistical weights) is much

less than 1%. Thus protonium, as a neutral system nearly the size of the hydrogen

atom having a thermal velocity of about 6×10^5 cm/sec, lives long enough (except

for the rare S-state annihilations) to make many collisions with hydrogen and

carbon atoms in the propane.

According to a recent paper by Day, Snow, and Sucher,[30] the l = 0

state of protonium (which annihilates) may become populated due to a Stark-effect

process. This process should occur very quickly for all m = 0 states whenever

the protonium is in a strong electric field. Such a strong field is encountered when

the protonium system is within the Bohr radius of a proton. Protonium has

about 2×10^{11} collisions per second with hydrogen atoms in propane. Because of

the statistical weight of the m = 0 states, some 30 collisions are necessary to reduce

the protonium by a factor of 1/e, assuming that the m values are reshuffled on

successive collisions. Thus we calculate that an approximate transition probability for protonium to annihilate (because of the Stark effect) is $21 \times 10^{11}/30$, or about 0.7×10^{11} sec^{-1}.

Protonium annihilation is not so likely to result from collisions with carbon atoms. The protonium atom is several times as big as the unscreened region of the carbon atom, hence only the proton or the antiproton may be within that region at a given time. For such a situation another process becomes very likely. This is the transfer of the antiprotons to carbon, in an effect similar to that observed for stopping π^- mesons by Panofsky and others.[31] Protonium makes about 1×10^{11} collisions per second with the unscreened region of a carbon atom in propane, and for these collisions we assume that the transfer efficiency per collision is high. Ignoring any additional transfer due to not-so-close collisions with carbon, we have a rough lower limit of 1×10^{11} sec^{-1} for the transfer rate of antiprotons from protonium to carbon.

By comparing the rate of protonium annihilation (due to the Stark effect) to the rate of transfer of antiprotons from protonium to carbon, and remembering that many of the antiprotons are originally captured by carbon, we can see that annihilations on carbon should be most frequent for antiprotons at rest. Furthermore, the occurrence of $\overline{p}$-H annihilations in any perceptible number must be considered to be due to the Stark effect acting on protonium.

We have evidence that the stopping antiprotons preferentially annihilate on carbon. We have found that for antiprotons of more than 75 Mev, the ratio of carbon to hydrogen annihilations is about 2. For all annihilations at less than 50 Mev, the ratio becomes 6, and for 71 antiprotons of longest range, the ratio is 12. We may go a step farther and explore the assumption that such a highly efficient transfer mechanism exists that all annihilations of stopped antiprotons occur on carbon nuclei. Such an assumption forces us to attribute the end-

of-the-range $\bar{p}$-p type annihilations to either (a) a sharp increase in the $\bar{p}$-p

annihilation cross section at low kinetic energy, or (b) a significant preponderance

of fake $\bar{p}$-p over fake $\bar{p}$-n stars. Consider Case (a): the assumption that $\bar{p}$-p

annihilations at the end of the range really occur at low kinetic energies (which

we cannot distinguish from zero) leads to $\sigma_{ann}(\bar{p}\text{-}p) = 455 \pm 105$ mb (0 to 75 Mev).

Such a large cross section is unlikely in view of the 1/v-law prediction of < 200 mb.

Let us then reject Case (a) and consider Case (b), in which we obtain a ratio of

1.8 ± 0.5 when comparing $\bar{p}$-n -type carbon annihilations with $\bar{p}$-p-type annihilations

at rest. This ratio is not at all inconceivable, but it is not in good agreement with

an expected ratio of 1.0.

We conclude that we have established that stopping antiprotons annihilate

preferentially on carbon in propane, which is expected. It is even possible that

the stopped antiprotons annihilate wholly on carbon, but this hypothesis leads to

conclusions that are not entirely satisfactory. Indeed, our results are in best

agreement with the annihilation of about 10% of all stopping antiprotons on hydrogen,

which is reasonably explained by the Stark-effect process.

C. Antiproton Polarization

In the design of the experiment, the possibility that carbon might be a good analyzer was acknowledged, even though no mechanism for antiproton polarization in production has been suggested. Antiprotons of 970 Mev/c initial momentum observed here were produced on a beryllium target by 6.1-Bev protons. Their angle of production was 5 deg left (lab), which corresponds to 169 deg (c.m.). Any polarization at production is expected to survive energy degradation.

The observed right-left asymmetry of the $\bar{p}$-C scatterings within 45 deg of the horizontal plane was $e_{R-L} = 0.12 \pm 0.17$, while an up-down asymmetry of $e_{U-D} = 0.18 \pm 0.15$ was obtained. These results are consistent with zero polarization in antiproton production. We cannot determine whether this negative result is due to a real absence of polarization in the antiproton beam, or whether it is due to the lack of analyzing power in carbon scattering (the analyzability is theoretically estimated to be only about 0.2)

V. RESULTS: THE ANNIHILATION PROCESS
A. Observation of Annihilation Products

Reports published previously have described the annihilation process
in nuclear emulsions[7,8] and in a bubble chamber.[10] In this experiment we
have observed some 500 annihilations. Detailed measurements were possible
on 437 annihilations, of which 140 fit requirements of annihilation on hydrogen.
The remaining 297 annihilations, all of which can definitely be attributed to
carbon, fall into two approximately equal groups: those which appear to occur after
the antiproton has come to rest (or has at most 50 Mev kinetic energy), and those
in which the antiproton still has significant kinetic energy (at least 50 Mev)
upon fatal collision with a carbon nucleus. Both the hydrogen and the carbon
annihilations are discussed in detail in the following sections.

The characteristic nucleon-antinucleon annihilation proceeds through
the creation of pions, both charged and neutral. In about 4% of the annihilations
at low antiproton kinetic energy, a pair of K mesons is created. No other
direct product has yet been observed.

We have used various methods to observe the various kinds of annihilation
products.

Protons and Charged Pions

The pion products from a fundamental N-$\bar{\text{N}}$ annihilation within a carbon
nucleus may interact before getting out of the nucleus. Such an interaction may give
rise to protons, neutrons, and other nuclear fragments. The charged prongs from
these stars are directly observable in the chamber and in many cases may be
identified on the basis of momentum, charge, and density of track. Distinction
between pions and protons is usually straightforward, except in rare cases of
high-momentum positive tracks. When dealing with the black prongs (i.e.,
heavily ionizing), however, we are unable to distinguish between short-range

protons and deuterons or other charged nuclear fragments. For convenience, all these heavy prongs are assumed to be protons.

A charged prong is considered identified once it has been designated as a π^+, a π^-, or a heavy prong (p^+). As we pointed out in Section II D, such a designation is made only after the scanner's tentative identification, based on bubble-count ionization measurements, is confirmed by the measured momentum.

Charged-particle identification breaks down for steep tracks. Here the momentum of the particle may be parallel to the magnetic field, so that not even the sign of the charge can be determined. Furthermore, even a minimum track looks dense in a projected view because the cameras are above the chamber. We have used two approaches to this problem:

(a) A compilation of all completely identified stars was made. Then each annihilation with one or more prongs undetermined was compared with the list of known stars. An assignment of particle identity (pion or proton) or particle charge (for pions only) was made in ratio to the frequency among the known stars of the various possible final configurations of the unknown star. To gain an idea of the numbers involved, consider the carbon annihilation at rest. In these 65% of the annihilations had complete prong identification,[34] 75% had no unidentified particle, and 80% had no unidentified charge. Furthermore, 90% of the prongs in this group of annihilations were identified.

(b) A compilation was made of all annihilation products, listing total number identified for each kind of particle. A separate listing was made for prongs of dubious identity or charge. These latter, amounting to 10% of all the prongs, were then assigned in blocks according to the over-all frequency of identified particles, without regard for specific stars. The result obtained was an average multiplicity of π^+, π^-, and p^+ for the group of stars under consideration. This process was repeated, using only those annihilation products

having dip angles within 30 deg of the horizontal. This region constitutes half the solid angle. Elimination of steep dip angles permits more confident identification of particles, and only 5% of all prongs in this sample were undetermined. Multiplicities determined in this way were in good agreement with those obtained for the whole solid angle and with those obtained by the method of detailed correction described in (a) above.

Detection efficiency for charged pions was about 99%. This estimate is based in part on a scanning-efficiency calculation based on the results of the two independent scans, and in part on the consideration of the two effects that can render pions unobservable. One of these effects is pion charge exchange or absorption near the annihilation origin, while the other is antiproton annihilation so close to the chamber top or bottom that particles can go out unobserved. Both effects together account for about 0.5% of the charged pions. The other common pion interactions, namely elastic scattering and pion decay, still allow the pion to be detected. Even for pion decay at rest near the annihilation, the characteristic $\pi \to \mu \to e$ decay scheme is easily identified through the 3-mm range of the μ meson and the usually visible (at least 98% of the time) electron.

Neutral Pions and Other Neutral Products

Uncharged annihilation products may occasionally be observed. The decay of neutral K mesons within a few centimeters of the annihilation makes detection extremely probable for the mode of decay in which two charged particles appear. This is discussed more fully in a subsequent section.

Neutrons ejected from carbon stars, however, are essentially undetectable because their reactions with charged particles, such as n-p elastic scattering, do not allow unique association with the annihilation. No attempt was made to obsdrve neutrons from annihilations.

Neutral pions may be observed infrequently through the pair conversion of a photon decay product. The number of neutral pions is related to the number of observed electron-positron pairs through two factors, the mean free path for pair production in the propane and the chamber geometry. The mean free path for pair production is a function of the energy of the photon, varying from 200 g/cm^2 (480 cm) of propane at 20 Mev to 64 g/cm^2 (154 cm) at 1000 Mev. The problem of chamber geometry was solved by establishing an arbitrary fiducial volume within the chamber. This volume was a rectangular parallelopiped slightly smaller than the chamber, and contained all the annihilations. Only photons that converted within this volume were accepted. Each observed pair was weighted by a factor $1/[1 - \exp(-l_v/l_p)]$, where l_p is the mean free path for photon conversion into a pair of the observed energy, and l_v is the distance from the annihilation to the fiducial-volume boundary along the photon line of flight. The observed electron pairs were corrected for energy loss before calculation of the weighting factor.

From the results of the two independent scans, we concluded that the scanning efficiency for pairs within the fiducial volume was 98.5%. About 7% of all the π^0-decay photons converted into pairs within the volume. This means that our π^0-detection efficiency was 14%.

A check for possible "accidental" pairs was made by scanning a section of film for pairs that appeared to originate from an arbitrary point near the center of the bubble chamber. This check indicated that approximately 2% of the observed annihilation-associated pairs should be accidental. Both this factor and the scanning-efficiency factor, which tend to balance each other, are considered negligible.

Dalitz Pairs

A consideration of annihilation products would not be complete without some reference to Dalitz pairs. In one of 80 π^0 decays, a photon materializes

directly as an electron-positron pair. These electron pairs look like direct
annihilation products, because the π^0 lifetime, $\tau < 4 \times 10^{-16}$ sec,[33] does not
allow physical separation of the pair origin from the annihilation origin in the
bubble chamber. If the electron path length is long enough -- e.g., at least 10 cm --
then an experienced scanner may recognize it by its high rate of energy loss
(radiation loss by an energetic electron). A low-energy electron is easily rec-
ognized by its characteristic spiral stopping.

Among the products of almost 500 annihilations, we have tentatively
identified 6 Dalitz pairs. If we assume that each annihilation produces 1.6 neutral
pions and that, of these, 0.2 is absorbed in each carbon star, then we should expect
to see 9 Dalitz pairs. This is considered satisfactory agreement with observation.

K Mesons

The strange-particle K-meson products of annihilation are discussed in
Section V D.

B. The Hydrogen Annihilation

In this section we present the result of measurements made on 140 stars
that meet the conditions for antiproton annihilation in hydrogen. It is estimated that
about 40 of these events are actually annihilations on carbon nuclei. Because it is
impossible to determine which hydrogenlike annihilations are genuine and which are
not, all are included in a single group considered typical of the $\bar{p}$-H annihilation.[34]
For these annihilations, the average kinetic energy of the antiproton was 80 Mev.

The multiplicity of charged mesons per hydrogen annihilation was found
to be 3.06 ± 0.12.[35] The average energy (including rest energy) was 390 ± 14 Mev
per charged meson. We have also observed 29 gamma-ray pair conversions which
give 1.6 ± 0.5 neutral pions per annihilation. The π^0 total energy averaged 356 ± 110
Mev. Combining, we have an observed multiplicity of 4.7 ± 0.5 pions per annihilation.

In addition, some 4% of these annihilations produced K mesons (see Section V D
for a discussion of strange particles produced by annihilations).

The error in our observed pion multiplicity of 4.7 ± 0.5 pions per anni-
hilation is mostly due to the large error in the neutral-pion multiplicity. If we
consider only charged pions, we may still calculate a combined charged-and
neutral-pion multiplicity if we make two assumptions: (a) the neutral pions have
the same average total energy (390 ± 14 Mev) as the charged pions, and (b) all the
annihilation energy that does not appear in K mesons is carried off by pions. Using
these assumptions, we get a pion multiplicity of 4.88 ± 0.18 pions per annihilation.
By subtracting the observed charged-pion multiplicity of 3.06 ± 0.12 from 4.88 ± 0.18,
we get a difference of 1.82 ± 0.21 pions per star that can be attributed to neutral pions.
These results are consistent with the production of equal numbers of π^+, π^-, and π^0
mesons, although such a division is not specifically required for $\bar{p}$-p annihilations.

The kinetic-energy spectrum of the observed charged pions is presented
in Fig. 7. Only those pions that make an angle of at least 60 deg with the magnetic
field and that have at least 10 cm of measurable track (unless stopping) are included.
Only 99 of the π^+ mesons meet these conditions (Fig. 7a). The average π^+ kinetic
energy is 240 ± 19 Mev. Eighty-six of the π^- mesons are recorded in Fig. 7b.
The average π^- kinetic energy is 263 ± 21 Mev. The most probable kinetic energy
for both π^+ and π^- is approximately equal to the pion rest mass, giving a most
probable total energy of about twice the pion rest mass.

Figure 8 shows an energy distribution of photon pair conversions. These
photons are decay products of π^0 mesons created in the hydrogenlike annihilations.
Each photon represented in Fig. 8 has been weighted according to its probability of
converting within the chamber. For a π^0 kinetic-energy spectrum similar to the
π^+ or π^-, the most probable γ energy is half the π^0 rest mass, or 68 Mev. Our
most probable value seems to be more than 100 Mev, but we must acknowledge the
poor statistics. When all photons, including those from carbon annihilations (see
next section), are considered, the resulting energy spectrum shows good agreement

with the predicted value of 68 Mev.

The over-all results for hydrogenlike annihilations are presented in Table VI. A more detailed breakdown is presented in Table VII. The data show that the hydrogen annihilation produces four charged mesons in about 50% of the events, while 40% have only two charged mesons. The remaining 10% is almost equally split between 0-prong and 6-prong stars. The π^0 multiplicity decreases as the $\pi^\pm$ multiplicity increases. With poor statistics, we find $2.4^{+1.2}_{-0.9}$ neutral pions per two-prong star, and $1.1^{+0.9}_{-0.5}$ per four-prong star.

Our results should be compared to the hydrogen bubble-chamber results of Horwitz, Miller, Murray, and Tripp,[10] who have studied 81 antiproton annihilations at rest. They have found 3.21 ± 0.12 charged mesons per annihilation. Their average for the $\pi^\pm$ energy (including rest mass) was 380 ± 12 Mev per pion. In other respects there is also good agreement. For example, they have also reported that 50% of the hydrogen annihilations have four prongs, while about 40% have two prongs.

It is also of interest to compare our results with the predictions of the several theories. The Fermi statistical model has been discussed extensively elsewhere in connection with antinucleon-nucleon annihilation.[7,8,10,11] The straightforward application of the Fermi theory predicts a low pion multiplicity (3.3 pions per annihilation when K production is ignored, and even fewer when K production is considered) and a high K probability (as much as 41%). The Fermi model can be brought into agreement with experimental results of almost five pions per annihilation by increasing the interaction volume $\Omega = 4/3 \, \pi \, (\hbar/m_\pi c)^3$ by a factor of ten, but even then the theory predicts about three times as many K mesons as were observed. Attempts to improve this theory by minor changes have so far been unsuccessful. As discussed by Sudarshan, Landau, and Pomeranchuk[36] enhancement of pion multiplicity can be obtained by considering a strong pion-pion interaction.

Table VI

Annihilation product	Average multiplicity	Energy per particle[a] (Mev)	Energy per annihilation (Mev)
Charged pions	3.06 ± 0.12	390 ± 14	1195 ± 62
Neutral pions[b]	1.6 ± 0.5	356 ± 110	570 ± 250
K mesons	0.08 ± 0.02	606 ± 77	49 ± 15
			1814 ± 258 (total)

Summary of hydrogenlike annihilations, based on 139 events

[a]Includes rest mass.
[b]Neutral-pion results appearing in this table were obtained by observation (through pair production) of about 7% of the decay photons. The π^0 multiplicity becomes 1.82 ± 0.21 if we assume that the average π^0 energy is the same as for charged pions.

Table VII

Breakdown of hydrogenlike annihilations

Five events in which K mesons were produced are excluded

Charged-pion multiplicity	Number of events	Energy per charged pion[a] (Mev)	Number of photon pairs	Neutral-pion multiplicity	Energy per neutral pion[a] (Mev)
0	8	---	3	(~3.5)[b]	*
2	54	424	15	$2.4^{+1.2}_{-0.9}$	365
4	67	378	10	$1.1^{+0.9}_{-0.5}$	330
6	6	310	1	(~1)[b]	*

[a]Includes rest mass.

[b]Small number of observed photons allows only a rough estimate.

*Statistics too poor to give a number.

The theory of Koba and Takeda suggests that annihilation pions have two distinct origins: first, the meson cloud, which gives 2.6 pions; and second, the nucleon core, which adds 2.2 pions. This model is based on the idea that periods of motion in the pion cloud are long compared with the core-annihilation time. Upon overlap of nucleon-antinucleon cores, annihilation proceeds nonadiabatically with respect to the pion periods. The reduced energy available to core annihilation is treated with the Fermi theory. The model predicts 4.8 pions per annihilation, which is in good agreement with the experimental results. However, recent calculations by Frautschi[37] indicate that the K-multiplicity predictions of the Koba-Takeda model are too high by a factor of about 4.

C.   The Carbon Annihilation

Description of the Carbon Star

We have divided all the antiproton annihilations in carbon into two groups: those which occur in flight, and those which occur at rest. An antiproton kinetic energy of 50 Mev was picked as a dividing line, and all antiproton annihilations at less than 50 Mev were considered at rest. In the energy region from 50 Mev to 200 Mev, 151 antiprotons of 120-Mev average kinetic energy annihilated with products that clearly identified the event as occurring on a carbon nucleus. As pointed out earlier, a correction must be made for carbon annihilations that are indistinguishable from hydrogen stars. Using the method described in Section III D, we estimate that 15 "fake" $\bar{p}$-H annihilations should be added to the identified carbon stars, to give a total of 166 in-flight carbon annihilations. Similarly, we have identified 146 carbon annihilations at rest and apply a correction of 25 fake $\bar{p}$-H stars to obtain a total of 171 at-rest carbon annihilations.

We have carried out a parallel analysis on the two groups of carbon annihilations. All the tables listing results compiled from the carbon stars

have separate columns for in-flight and at-rest events. All graphs and plots are duplicated in a like manner, so that a glance at a single figure allows quick comparison between similar quantities derived from at-rest and in-flight annihilations.

The products from carbon stars are pions and particles giving heavy prongs. For convenience, all the heavy prongs have been classified as protons, with a lower cutoff of 10 Mev, which corresponds to a proton range of 2 mm. The annihilation multiplicities for the in-flight stars are 1.65 ± 0.09 π^- per star, 1.31 ± 0.10 π^+ per star, 1.16 ± 0.40 π^0 per star, and 1.58 ± 0.10 p^+ per star. For the at-rest annihilations, we get 1.50 ± 0.10 π^- per star, 1.35 ± 0.12 π^+ per star, 1.14 ± 0.40 π^0 per star, and 1.03 ± 0.08 p^+ per star. These results are also shown in Table VIII. The combined total pion multiplicity, charged plus neutral, is seen to be about 4.1 ± 0.3 pions per star. This is significantly less than the 4.7 ± 0.5 pions observed in hydrogen annihilations, and this difference as well as other features of the carbon annihilation is discussed in the following section.

The kinetic-energy spectra for positive and for negative pions produced in these carbon annihilations are given in Fig. 9. As in the hydrogen annihilation, only those pions which had 10 cm of measured path (unless stopping) and which made an angle of at least 60 deg with the magnetic field were included in the energy spectra. These same conditions were applied to get the proton energy spectra shown in Fig. 10. The average kinetic energies from the inflight annihilations were as follows: 86 π^+ gave $\langle \vec{T} \rangle = 242 \pm 19$ Mev, 106 π^- gave $\langle \vec{T} \rangle = 215 \pm 17$ Mev, and 136 p^+ above a 10-Mev cutoff gave $\langle \vec{T} \rangle = 68$ Mev. Average kinetic energies from the at-rest annihilations were as follows: 86 π^+ gave $\langle \vec{T} \rangle = 223 \pm 18$ Mev, 101 π^- gave $\langle \vec{T} \rangle = 239 \pm 19$ Mev, and 76 p^+ above a 10-Mev cutoff gave $\langle \vec{T} \rangle = 75$ Mev.

Table VIII

Multiplicities and energies of the principal products of carbon annihilations

| Product | In-flight stars 166 events | | At-rest stars 171 events | | Combined 337 events | |
	Multi-plicity	Energy[a]	Multi-plicity	Energy[a]	Multi-plicity	Energy[a]
π^-	1.65±0.09	354±17	1.50±0.10	378±19	1.58±0.07	366±13
π^+	1.31±0.10	381±19	1.35±0.12	362±18	1.33±0.08	371±13
π^0	1.16±0.40	342±120	1.14±0.140	343±120	1.15±0.30	342±90
$p^{+(b)}$	1.58±0.10	68	1.03±0.08	75	1.29±0.07	71

[a] Total energy is given for pions, kinetic energy for protons.

[b] This includes all heavy charged particles with propane range greater than 2 mm, which is the range of a 10-Mev proton. See Fig. 10 for the p^+ energy spectrum.

The photon energy spectra arising from π^0 decays are given in
Fig. 11. Twenty-three photon-produced pairs were measured to produce
the plot associated with in-flight annihilations, while 25 pairs were associated
with the at-rest annihilations. The weighted average energy for both types of
annihilation was 171 Mev per pair, giving an average π^0 total energy of
342 ± 120 Mev.

A detailed breakdown of the carbon annihilations is given in Table IX.
Here the annihilations are classified according to the number of heavy prongs.
For example, all annihilations that produced only one black prong, regardless
of its energy, are treated as a separate group. Groups were set up for anni-
hilations with 0, 1, 2 and >2 black prongs. A final group--really a subgroup
of the group with one black prong--included only stars with purely pionic
products except for one energetic proton $(T > 40$ Mev). Pion multiplicities and
energies are given for each group. In some cases, the number of events is too
small to give statistically meaningful results, particularly for neutral pions.

The distribution of annihilations according to the total number of
charged prongs from the stars is shown in Fig. 12. A more informative
prong-frequency distribution in which only the pions are considered is given
in Fig. 13. This pion-frequency distribution is also given in Table X, in which
the π^0 multiplicity is included, showing the decrease in π^0 mesons along with
an increase in the number of charged pions. This was also noticed in the
hydrogen annihilation.

The distribution of carbon annihilations according to the net charge
of their pion products is presented in Table XI. All heavy prongs were ignored
in preparing this table. It is seen that most annihilations have a net pionic
charge of either $\Sigma q = 0$ or $\Sigma q = -1$. This is to be expected for simple $\bar{p}$-p or
$\bar{p}$-n annihilations. However, 25% of the carbon annihilations have $\Sigma q \neq 0$ or
$\Sigma q \neq -1$. Another interesting fact is that the surplus of negative charge is only
0.25 π^- per annihilation. An interpretation of these data, leading to conclusions

Table IX

Multiplicities and energies of the principal products of several types of carbon annihilation

Type of annihilation	Product	In-flight stars		At-rest stars		Combined	
		Multi-plicity	Energy (Mev)	Multi-plicity	Energy (Mev)	Multi-plicity	Energy (Mev)
$\bar{p}$-C stars with no heavy prong	π^-	1.74	370	1.67	369	1.70	369
	π^+	1.47	379	1.43	363	1.45	370
	π^0	1.60	484	1.60	378	1.60	431
	p^+	0	--	0	--	0	--
		38 events		72 events		110 events	
$\bar{p}$-C stars with one heavy prong	π^-	1.73	344	1.57	387	1.65	364
	π^+	1.50	381	1.28	339	1.40	361
	π^0	0.83	322	0.70	272	0.77	300
	p^+	1.0	--	1.0	--	1.0	--
		52 events		46 events		98 events	
$\bar{p}$-C stars with two heavy prongs	π^-	1.47	341	1.26	384	1.38	358
	π^+	1.30	349	1.33	417	1.31	378
	π^0	1.00	336	1.23	312	1.10	326
	p^+	2.0	--	2.0	--	2.0	--
		36 events		27 events		63 events	
$\bar{p}$-C stars with more than two heavy prongs	π^-	1.61	333	1.48	341	1.56	336
	π^+	1.00	427	1.32	316	1.12	377
	π^0	1.30	258	0.60	284	1.03	264
	p^+	3.7	--	3.4	--	3.6	--
		41 events		25 events		66 events	
$\bar{p}$-C stars with one energetic proton ($T_{p^+} > 40$ Mev)	$\pi^\pm$	3.18	--	2.24	--	2.71	--
	π^0	1.60	--	1.24	--	1.42	--
	p^+	1.00	83	1.00	98	1.00	90
		17 events		17 events		34 events	

Table X

Pion-frequency distributions observed in $\bar{p}$-C annihilations [a]

Number of charged pions	In-flight stars		At-rest stars		Combined	
	Number of stars	π^0 multi-plicity	Number of stars	π^0 multi-plicity	Number of stars	π^0 multi-plicity
0	2	(~2)	3	(~2)	5	(~2)
1	23	2.0	25	2.6	48	2.3
2	37	1.4	39	1.2	76	1.3
3	47	1.8	51	1.2	98	1.5
4	37	0.2	33	0.5	70	0.4
5	15	-	17	-	32	-
6	4	-	2	-	6	-
7	1	-	0	-	1	-

[a] All heavy-prong annihilation products were ignored in compiling these data.

Table XI

Distribution of carbon annihilations according to net charge of their pion products

Net charge	In-flight stars	At-rest stars	Combined	Predicted
-3	1	0	1	2
-2	10	5	15	22
-1	62	64	126	132
0	64	67	131	130
+1	24	26	50	46
+2	5	9	14	5
+3	0	0	0	0

about the $\bar{p}$-p and $\bar{p}$-n annihilation ratio within the carbon nucleus, is given in the next section.

A carbon annihilation of especial interest is the neutron-type annihilation. We have observed 40 annihilations on carbon nuclei which simulate free $\bar{p}$-n annihilations. These events, all of which were purely pionic and had an excess of one negative pion, were divided as shown in Table XII. The charged-pion multiplicity was 3.25 ± 0.25 $\pi^{\pm}$ per annihilation. The average energy per pion was 362 ± 24 Mev, including the $\pi^{\pm}$ rest mass. Eleven gamma-ray-pair conversions (five on 3-prong stars and six on 1-prong stars) gave $1.8^{+1.1}_{-0.7}$ π^0 per annihilation. The π^0 total energy averaged 444 ± 197 Mev. Combining the charged and neutral pions, we get $5.05^{+1.1}_{-0.7}$ pions for a total of 1976 Mev per annihilation (one event giving K mesons was excluded). The above results may be regarded as giving an indication of the details of the $\bar{p}$-n annihilation.

A breakdown of the energy observed from carbon stars is presented in Table XIII.

<u>Interpretation of the Carbon Star</u>

<u>Pion absorption</u>. The first notable characteristic of the carbon annihilation is that the pion multiplicity is less than that observed in hydrogen. This decrease is not regarded as likely to be due to a significant difference in the primary nucleon-antinucleon annihilation, but is attributed to absorption of pions by the residual nucleus. This interpretation is borne out by the presence of the heavy prongs.

Heavy prongs from a carbon annihilation might have five different origins:

(a) The absorption of an annihilation pion in the residual nucleus. This is pictured as a three-body interaction--the inverse of the pion production reaction $N + N \rightarrow \pi + N + N$.

(b) The inelastic[38] or charge-exchange scattering of one of the annihilation pions on one of the residual nucleons.

Table XII

Charged-pion multiplicity	Number of events
1	9
3	18
5	12
7	1

Charged-pion multiplicity in neutronlike annihilation

Table XIII

Breakdown of the energy observed from carbon stars

	In-flight stars	At-rest stars
Energy expected (Mev)	1996	1876
Energy observed (Mev)		
π^-	584 ± 42	566 ± 47
π^+	500 ± 45	488 ± 50
π^0	397 ± 197	391 ± 188
Nucleons	>212	> 164
K	49 ± 15	49 ± 15
Total observed	>1742 ± 207	> 1658 ± 200

(c) The quasi-elastic scattering of a proton by an antiproton which subsequently annihilates in the same nucleus.

(d) The evaporation of nucleons from an excited residual nucleus.

(e) An annihilation that possibly involves directly two or more nucleons, wherein nucleons or nuclear fragments may obtain annihilation energy without an intermediate state of real pions.

Only the first two processes are regarded as important to the explanation of observed multiplicities and energies of the pions. Evaporation prongs (Process (d)) can appear in association with any of the other interactions, and no serious effort will be made to investigate them. Processes (c) and (e) are ignored.[39]

Processes (a) and (b) can be pursued further on the basis of a very simplified approach. We assume that a pion interacts only once before leaving the nucleus. This assumption is justified on the grounds that the mean free path for scattering in nuclear matter is greater than the nuclear radius except at the π-N resonance. Moreover, the assumption is supported by the report that for π^- incident on carbon nuclei (in great contrast to heavier nuclei), the angular distribution for inelastic scattering is similar to that expected for scattering on free nucleons.[40]

We have taken the mean free paths for pion scattering and absorption in nuclear matter as a function of energy[41] and weighted them according to our observed energy spectrum of pions from hydrogen annihilations. This gives us the relative number of pions scattered and absorbed as a function of pion energy. We estimate from these calculations that absorption occurs half as often as scattering, and that the average kinetic energy of the absorbed pion is $\langle T \rangle$ = 315 Mev, whereas for scattering the average is $\langle T \rangle$ = 240 Mev.

An absorption of a pion at $\langle T \rangle$ = 315 Mev should release $T + M_\pi$ = 454 Mev to the nucleons involved. Furthermore, since the absorption occurs

preferentially at high pion energies, the observed pion-energy spectrum will be altered by their disappearance.

Further calculations show that the average change in kinetic energy of of a pion in a scattering process is $\langle \Delta T \rangle = -60$ Mev. This has been weighted over the pion energy spectrum and averaged over the scattering angular distribution.

Combining the absorption and scattering in the ratio of two scatterings per absorption, we expect that 80% of the energy given to nucleons is due to pion absorption. This energy can not all be observed directly because neutrons, which are assumed to carry off half the energy, are invisible, and also because of unobserved black prongs shorter than our 2-mm cutoff. Thus we may only place a lower limit on the energy per star carried off by nucleons. We have the following situation for carbon stars:

	in flight	at rest
energy in black prongs per star	> 106 Mev	> 82 Mev
energy in nucleons per star	> 212 Mev	> 164 Mev

We may now compute the pion multiplicities for carbon stars, after correcting for absorption and scattering. These are:

	in flight $(\langle T_{\bar{p}} \rangle = 120$ Mev)	at rest
pion multiplicity (observed)	4.1 ± 0.4	4.0 ± 0.4
energy in nucleons per star	> 212 Mev	> 164 Mev
pion multiplicity (corrected)	> 4.5 ± 0.5	> 4.3 ± 0.5

These numbers should be compared with a pion multiplicity of 4.7 ± 0.5 at $\langle T_{\bar{p}} \rangle$ = 80 Mev for our hydrogen annihilations.

Another way to determine the pion absorption in carbon is to consider the pion energy spectra in carbon and hydrogen. Because the errors on π^0

energies are large, we consider only the charged pions for comparison. All carbon annihilations give average total energy $\langle E \rangle$ = 368 ± 9 Mev per charged pion, while the hydrogen annihilations give $\langle E \rangle$ = 390 ± 14 Mev. With our crude model wherein absorption occurs half as often as scattering, a 22-Mev change in average pion energy is expected when 0.5 pion is absorbed per carbon annihilation.

We conclude that the pion absorption in carbon amounts to ~0.6 pion per annihilation, which is obtained by subtracting the directly observed carbon multiplicity of 4.1 from the hydrogen multiplicity of 4.7. This absorption of ~0.6 pion per annihilation is confirmed by the energy observed in black prongs (which is consistent with >0.4 pion absorbed) and with the observed average pion energy (which is consistent with 0.5 pion absorbed). We further conclude that our assumption that the primary N-$\overline{N}$ annihilation within the carbon nucleus has the same products as a free N-$\overline{N}$ annihilation is essentially correct.

In-flight vs at-rest stars.   The mean free path for antiprotons in nuclear matter is about 0.6×10^{-13} cm at 100 Mev. [42] This means that nearly all annihilations occur on the nuclear surface. Previous reports, based on emulsion studies, have suggested that significant differences between in-flight and at-rest black-prong multiplicities stem from the surface annihilation of at-rest antiprotons as contrasted with the deeper nuclear penetration of more energetic antiprotons. [7,8] An alternative explanation of in-flight and at-rest differences is based on a feature of the annihilation in flight that has escaped comment heretofore.

We have observed that, for in-flight carbon stars, black prongs are more frequent and that more energy appears in nucleons, suggesting a difference in pion absorption. But we have also observed an expected forward-backward asymmetry (due to center-of-mass motion) in pions produced by in-flight annihilations. This observed asymmetry indicates that 1.4 pions emerge in the forward hemisphere for each one emerging backward at $\langle T_{\overline{p}} \rangle$ = 120 Mev in

carbon. We expect that 1.8 pions are produced forward for each one produced
backward, before absorption. We assume now that annihilation occurs at a depth
such that the effective solid angle subtended by the nucleus approaches 2π (i.e.,
occurs near the nuclear surface). Annihilations in flight occur near the front
surface of the nucleus, and the center-of-mass motion causes more of the pions
to traverse the nucleus in these annihilations than in at-rest annihilations. We
further assume that the 120-Mev average kinetic energy (lab) of the incident anti-
proton should cause an increase of ~0.15 pion in the observed multiplicity. [43]
These two assumptions lead to a predicted difference in pion absorption that almost
accounts for the energy observed in nucleon products for in-flight and at-rest
carbon stars. Probably the only conclusion that can be derived from this result
is that really significant differences in carbon nucleus penetration do not occur
for in-flight and at-rest annihilations. This implies that the mean free path for
antiproton annihilation in nuclear matter remains short (less than a fermi) for
energies up to 200 Mev.

Pion net-charge distribution. It was pointed out in the preceding section that
most annihilations in carbon have a net pion charge of either $\Sigma q = 0$ or $\Sigma q = -1$.
This is expected on the basis of simple $\bar{p}$-p and $\bar{p}$-n annihilations within the carbon
nucleus, followed by pion charge exchange and absorption reactions that obey
charge independence.

        Actually, even with equal $\bar{p}$-p and $\bar{p}$-n annihilation cross sections, we
do not expect the difference in average multiplicity to be $n(\pi^-) - n(\pi^+) = 0.5$
(which would obtain for free protons and neutrons), for the following reasons:
Pion absorption alone, assumed equally probable for charged and neutral pions,
reduces the π^- excess to 0.43 π^- per carbon annihilation. Furthermore, an
original excess of π^- means that more π^- undergo charge exchange. Still another
process that reduces the expected π^- excess in carbon annihilations is the two-step

interaction $\bar{p} + p \rightarrow \bar{n} + n$ (in carbon) followed by $\bar{n}$ annihilation within the same carbon nucleus (this can even give a net pion charge $\Sigma q = +1$). After considering all these effects, we are able to calculate an expected pion net-charge distribution for the carbon annihilations. The calculation is based on the following assumptions: (a) $\bar{p}$-p and $\bar{p}$-n annihilations are equally probable within the nucleus, (b) the probabilities for the various modes for $\bar{p}$-p and $\bar{p}$-n annihilations are the same as given in Table VII and XII, (c) 0.6 pion is absorbed per star (absorption is assumed equally probable for π^+, π^-, and π^0), (d) 1.2 pions are scattered per star (all processes are assumed to occur in the $I = 3/2$ state), and (e) $\bar{p}$-p charge exchange with subsequent annihilation occurs 0.15 times as often as $\bar{p}$-n annihilation. The results of the calculation are given in Table XI. The predicted distribution gives a difference in average multiplicity of $n(\pi^-) - n(\pi^+) = 0.38$, and it fits the observed distribution with minor deviations.

We can summarize our results as follows:

Pion excess per annihilation	In flight	At rest	Combined	Predicted
$n(\pi^-) - n(\pi^+)$	0.34 ± 0.13	0.15 ± 0.15	0.25 ± 0.11	0.38

These results do not allow any emphatic conclusions. In particular, the discrepancies are not considered sufficient to alter our assumption of equally probable $\bar{p}$-p and $\bar{p}$-n annihilations within carbon, although the possibility of a difference is suggested by our at-rest data. Such a possibility has been suggested by Amaldi,[16] but must be verified by further experiment.

D. Strange Particles

The nucleon-antinucleon annihilation process is able to produce a pair of K mesons. This is predicted[44] as well as observed.[7] Our large propane chamber is highly efficient for the observation of short-lived neutral K mesons;

for an example, see Fig. 14. Charged K mesons can also be detected in long tracks under good ionization conditions, and of course, when they decay within the chamber. An example of K^+ decay at rest is shown in Fig. 15.

It should be pointed out that all strange particles (hyperons or K mesons) associated with an annihilation event can be assumed to result, either directly or indirectly, from the initial $\overline{N}N$ creation of a K-meson pair during annihilation. Other methods of producing strange particles are ruled out for reasons discussed in the next paragraph.

The production of a pair of K mesons by an annihilation pion is ruled out because of the high threshold energy required. One must also consider the reaction $\pi + N \rightarrow K + Y$, which might be expected to occur as the result of the interaction of a pion created in an annihilation and one of the residual nucleons in a carbon nucleus. Only about 2% of the pions created in an annihilation have sufficient energy to exceed the threshold for the case. Using a mean free path in nuclear matter of $\sim 2 \times 10^{-11}$ cm for the process, we arrive at the prediction that in all the $\bar{p}$-C annihilations reported here there should have been only about 1/2 an event.

Hyperons can be made in carbon annihilations via an indirect process. The exothermic reaction $K + N \rightarrow \pi + Y$ can occur within the same carbon nucleus as annihilation. Hence annihilation-produced K^- or $\overline{K}^0$ mesons may be converted into Λ^0 or Σ hyperons. Figure 14 contains a Λ^0 which is presumably an example of this process.

The same reaction, $K + N \rightarrow \pi + Y$, when it occurs within the chamber but at some distance from the annihilation, is sufficient to verify the identification of a K^- meson.

In our selected group of 436 annihilations, we were able to identify twelve as producing strange particles, and tentatively identify five others. These events

are listed and very briefly described in Tables XIV, XV, and XVI. We believe

that our scanning efficiency for $K_1^0 \to \pi^+ + \pi^-$ is practically 100%, since they

decay within a few centimeters of the annihilation, a region subjected to the closest

inspection. Scanning efficiency for the charged mesons is not greater than 70%.

This number is obtained by assuming all $K^{\pm}$ mesons with dip angle greater than

45 deg to be undetectable. Upon adopting this assumption we establish 45 deg

dip angle as a cutoff and ignore possible charged K mesons that have steeper angles.

We also assume that all charged K mesons with dip angles within the accepted

values are detectable. Above 150 Mev, this last assumption becomes risky, for

the K ionization drops below twice minimum.

Restricting ourselves to those twelve cases in which definite identification

could be made, we find four K_1^0 (including event No. 32327), seven K^+, four K^-,

and two Λ^0. For the four K_1^0 observed we make a correction for the 32%

branching ratio of the mode $K_1^0 \to \pi^0 + \pi^0$, which we cannot observe.[45] We

then again correct for the long-lived K_2^0 decays, giving us a total of 11.8 K^0

mesons. Still another correction should be made to the neutral K mesons to

account for the $\overline{K}^0$ absorption or hyperon production in the same nucleus as

annihilation occurs. Observation of two Λ^0 hyperons among the products of $\overline{p}$

annihilation in carbon indicates some three events (1/3 of the Λ^0 decay neutrally)

in which either a K^- or a $\overline{K}^0$ meson has interacted. We assume that 1.5 $\overline{K}^0$

and 1.5 K^- mesons have so interacted. This yields a total of 13.3 K^0 mesons.

Turning now to the charged K mesons, we apply our scanning correction

to the 7 K^+ and 4 K^- to get 10 K^+ and 5.7 K^-. We also add 1.5 K^- for interaction

in carbon nuclei for a total of 10 K^+ and 7.2 K^-, or 17.2 charged K particles in all.

Adding together charged and neutral K mesons, we find a corrected total

of 30.5 in 436 annihilations, which yields $3.5^{+1.0}_{-0.8}$ % of the annihilations giving

$K \overline{K}$ pairs. The error stated is statistical and based on the 17 observed events.

This result may be regarded as a lower limit. If we inspect the 17 events listed

Table XIV

Identified strange particles associated with antiproton annihilation

Event	Strange particle	Identification Method	$\frac{t}{\tau}$[a]	Kinetic energy at decay (Mev)	Kinetic energy at annihilation[b] (Mev)
22758	K^+	Ionization determination over 14 cm of track	-	--	74
28004	K^0	Good fit to annihilation orgin Good fit to decay kinematics	0.3	120	120
	Λ^0	Good fit to annihilation origin Good fit to decay kinematics	0.6	112	112
28432	$K^+_{\mu2}$	Elastic K^+-p scatter Ionization decrease upon forward decay Decay fits kinematics for $K_{\mu2}$	0.1	104	235
31375	K^-	A Λ^0 is produced by the star at end of track	-	0	33
	K^+	Ionization decrease upon forward decay of stopping particle. Kinematics uncertain but π-μ decay easily ruled out.	-	0	93
31395	K^+	Ionization determination over 11 cm of track	-	-	70
	K^-	A negative track of greater than minimum ionization makes a star of two pions with total visible energy 457 Mev. The two pions have momenta consistent with the production and subsequent decay of a hyperon.	-	0	26

(Continued)

Table XIV (continued)

Event	Strange particle	Identification method	$\frac{t}{\tau}$ [a]	Kinetic energy at decay (Mev)	Kinetic energy at annihilation[b] (Mev)
31978	K_1^0	This is a neutral K which fits annihilation origin.	0.1	187	187
32327	$K_{\pi2}^+$	Good fit to decay kinematics The pion decays in the chamber.	0.05	237	267
	V^0	Good fit to annihilation origin. The tracks are too steep to make momentum determination. Could be either a Λ^0 or $\bar{K}^0$.	-	-	-
32913	K^-	Track of greater than minimum ionization makes a star which produces well-verified Λ^0.	-	$0 < T \leqslant 94$	$30 \leqslant T \leqslant 100$
36046	$K_{\pi2}^+$	The track fits stopping K. The decay at rest agrees with $K_{\pi2}^+$ mode.	-	0	43
37270	K^-	Stopping negative particle has no charged products. A Λ^0 fits the ρ star.	-	0	46
44480	Λ^0	Good fit to annihilation point. Satisfactory fit to decay kinematics.	0.2	32	32
	K^+	Tentative, based on ioniza-tion in 11 cm of track	-	-	89

Table XIV (continued)

Event	Strange particle	Identification method	$\dfrac{t}{\tau}$ [a]	Kinetic energy at decay (Mev)	Kinetic energy at annihilation[b] (Mev)
45753	K_1^0	A neutral K which fits annihilation. One of the pions scatters and decay kinematics are not completely verified.	1.0	205	205

[a] The quantity $\dfrac{t}{\tau}$ is the ratio of the life of the particular particle with respect to its mean life.

[b] Kinetic energy of a strange particle upon leaving the point of antiproton annihilation.

Table XV

Tentatively identified strange particles

Event	Strange particle	Identification method	$\dfrac{t}{\tau}$	Kinetic energy at decay (Mev)	Kinetic energy at annihilation (Mev)
13324	Σ^+	Ionization decrease upon backward decay Identification of π-μ-e decay product.	2.3	83	92
22305	K^+	Determination of ionization in 12 cm of track	-	-	67
23060	K^+	Determination of ionization in 17 cm of track.	-	-	127
33554	Λ^0	Good fit to annihilation. origin. Measurement of momentum of the pion decay product is uncertain.	1.8	85	85
43349	K^+	Determination of ionization in 18 cm of track.	-	-	160

Table XVI

Information about annihilations in which strange particles are created

Event	Strange particles	Annihilation nucleus	Kinetic energy at annihilation (Mev)	Other visible annihilation products	Approximate missing energy (Mev)
Identified:					
22758	K^+	H	124	$2\pi^-$, $1\pi^+$, $1(\pi K)^{-a}$, $(p\pi)^+$	$0 < E < 400$
28004	$K^0 + \Lambda^0$	C	<50	$1\pi^-$, $1(p\pi)^+$, $2p^+$	$150 < E < 400$
28432	K^+	H	150	$1\pi^-$, $1\pi^+$, $1(\pi K)^-$	$0 < E < 300$
31375	$K^- + K^+$	C	71	$1\pi^+$, $2p^+$	500
31395	$K^- + K^+$	C	192	$1\pi^-$	600
31978	K_1^0	H	<50	$1\pi^-$, $2\pi^+$, $1(\Pi K)^+$	$0 < E < 300$
32327	$K^+ + V^0$	C	157	$1\pi^-$, $4p^+$	100
32913	K^-_+	H	<50	$1\pi^+$	1100
36046	K	C	0	$1(\pi K)^-$, $1(p\Pi)^+$	$500 < E < 1000$
37270	K^-	H	0	$1\pi^+$,	1100
44480	$K^+ + \Lambda^0$	C	0	$1\pi^+$, $1p^+$	800
45753	K_1^0	C	0	$1\pi^+$, $1(p\pi)^+$	$500 < E < 750$
Tentative:					
13324	Σ^+	C	169	$3\pi^-$, $1\pi^+$, $2p^+$	500
22305	K^+	C	0	$2\pi^-$, $2\pi^+$, $1p^+$	100
23060	K^+	C	140	$1\pi^-$, $1\pi^+$, $1p^+$	800
33554	Λ^0	C	108	$2\pi^-$, $2\pi^+$, $3p^+$, $1(pK)^+$	$-500 < E < 0$
43349	K^+	H	50	$1\pi^-$	900

[a] The symbol $(\pi K)^-$ indicates that a steep negative track was observed, but particle identification was not possible.

in Table XIV, we see eight particles with strangeness = +1, seven with $S = -1$. and two $K_1{}^0$, for which strangeness is undefined.

If we include the tentatively identified strange particles (Table XV) in our calculations, then we obtain the result that $4.5 \pm 0.9\%$ of the annihilations produce $K\overline{K}$ pairs.

In view of the uncertainties in scanning, and recognizing that some of the tentatively identified K mesons are probably valid, we feel that a best estimate is that $4.0 \pm 1.0\%$ of all annihilations produce $K\overline{K}$ pairs.

In Fig. 16 we present the kinetic energy spectrum of all the K mesons observed.

ACKNOWLEDGMENTS

We wish to express our appreciation to Mr. Larry Oswald, Lawrence Radiation Laboratory, and to Professor Louis Gilly, Centre de Physique Nucléaire, Université de Louvain, Heverle, Belgium, for help in this experiment. In addition the cooperation and help of Dr. Edward J. Lofgren and the staff of the Bevatron was greatly appreciated.

REFERENCES AND FOOTNOTES

1. Chamberlain, Segrè, Wiegand, and Ypsilantis, Phys. Rev. 100, 947 (1955).

2. Chamberlain, Keller, Segrè, Steiner, Wiegand, and Ypsilantis, Phys. Rev.
    102, 1637 (1956).

3. Cork, Lambertson, Piccioni, and Wenzel, Phys. Rev. 107, 248 (1957).

4. Agnew, Chamberlain, Keller, Mermod, Rogers, Steiner, and Wiegand,
    Phys. Rev. 108, 1545 (1957).

5. Chamberlain, Keller, Mermod, Segrè, Steiner, and Ypsilantis, Phys. Rev.
    108, 1553 (1957).

6. Button, Elioff, Segrè, Steiner, Weingart, Wiegand, and Ypsilantis, Phys. Rev.
    108, 1557 (1957).

7. Barkas, Birge, Chupp, Ekspong, Goldhaber, Goldhaber, Heckman, Perkins,
    Sandweiss, Segrè, Smith, Stork, and Van Rossum, and Amaldi, Baroni,
    Castagnoli, Franzinetti, and Manfredini, Phys. Rev. 105, 1037 (1957).

8. Chamberlain, Goldhaber, Jauneau, Kalogeropoulos, Segrè, and Silberberg,
    Phys. Rev. 113, 1615 (1959).

9. Coombes, Cork, Galbraith, Lambertson, and Wenzel, Phys. Rev. 112, 1303
    (1958).

10. Horwitz, Miller, Murray, and Tripp, Phys. Rev. 115, 472 (1959).

11. E. Segrè, Ann. Rev. Nuclear Sci. 8, 127 (1958).

12. J. Ball and G. Chew, Phys. Rev. 109, 1385 (1958).

13. S. Gartenhaus, Phys. Rev. 107, 291 (1957).

14. P. Signell and R. Marshak, Phys. Rev. 109, 1229 (1958).

15. Emilio Segrè, in Proceedings of Ninth Annual Rochester Conference on High-
    Energy Physics. Kiev. 1959.

16. Amaldi, Baroni, Bellettini, Castagnoli, Ferro-Luzzi, and Manfredini (Istituto di Fisica Dell'Universita, Roma, Italy and Istituto Nazionale di Fisica Nucleare, Sezione di Roma, Italy), private communication.

17. Z. Koba and G. Takeda, Progr. Theoret. Phys. (Kyoto) 19, 269 (1958).

18. Cork, Lambertson, Piccioni, and Wenzel, Phys. Rev. 104, 1193 (1956).

19. Agnew, Elioff, Fowler, Gilly, Lander, Oswald, Powell, Segrè, Steiner, White, Wiegand, and Ypsilantis, Phys. Rev. 110, 994 (1958).

20. Powell, Fowler, and Oswald, Rev. Sci. Instr. 29, 874 (1958).

21. J. R. Fulco, Phys. Rev. 110, 784 (1958).

22. J. S. Ball and J. R. Fulco, Phys. Rev. 113, 647 (1959).

23. The results of several groups at Berkeley, Los Alamos, Oxford, Rome, Saclay, and Uppsala, have been used for this compilation.

24. Agnew, Elioff, Fowler, Gilly, Lander, Oswald, Powell, Segrè, Steiner, White, Wiegand, and Ypsilantis, Phys. Rev. Lett. 1, 27 (1958).

25. F. Bjorklund and S. Fernbach, (Lawrence Radiation Laboratory, Livermore) and J. Fulco (Lawrence Radiation Laboratory, Berkeley), private communications.

26. The pair conversion of π^0-decay photons in the propane bubble chamber is discussed at some length in Section VA.

27. On the assumption that the carbon and hydrogen cross sections are equal, we get $\sigma \leq 11$ mb. The suggestion by Button et al. of the possibility of equal cross sections is reported in Reference 2.

28. I am indebted to Professor Robert Serber of Columbia University for some very useful comments on the $\bar{p}$-capture process at rest in propane. The capture of negative particles stopping in chemical compounds is discussed by E. Fermi and E. Teller, Phys. Rev. 72, 399 (1947).

29. H. Bethe and J. Hamilton, Nuovo cimento 4, 1 (1956).

30. Day, Snow, and Sucher, Phys. Rev. Lett. 3, 61 (1959).

31. Panofsky, Aamodt, and Hadley, Phys. Rev. 81, 565 (1951).

32. It would clearly be incorrect to report on only this 65%, because they are not representative of all the annihilations. The undetermined prongs occur most frequently in stars of high multiplicity.

33. Orear, Harris, and Taylor, Bull. Am. Phys. Soc. 2, 6 (1957).

34. To justify this, we inquire how much energy is carried off by unobserved neutrons. Energetic neutrons from carbon stars must be expected to have about the same energy distribution as energetic protons, which we can observe. Even if each of the $\bar{p}$-p stars has one energetic neutron, which is a very pessimistic estimate, the average energy per hydrogenlike annihilation available to pions is reduced by only 1.5%.

35. The charged-meson mean multiplicity, M, is given by $M = \dfrac{\Sigma_i \, i n_i}{\Sigma_i \, n_i}$,

where n_i is the number of annihilations having i charged mesons. The error in M is given by $\Delta M = \left[\Sigma_i \left(\dfrac{\partial M}{\partial n_i} \right)^2 (\Delta n_i)^2 \right]^{1/2}$, where Δn_i is the statistical error on n_i.

36. G. Sudarshan, Phys. Rev. 103, 777 (1956); L. Landau, Izvest. Akad. Nauk USSR 1: 51 (1953); I. Pomeranchuk, Doklady Akad. Nauk USSR 78, 88 (1951).

37. S. Frautschi (Research Institute for Fundamental Physics, Kyoto University, Kyoto, Japan), private communication.

38. The scattering is inelastic because it occurs in the presence of the nucleus. Process b is intended to be the inside-the-nucleus version of $\pi + N \rightarrow \pi + N$.

39. Another interaction ignored in this paper is the production of pions by pions, which becomes important at energies above 500 Mev.

40. S. J. Lindenbaum, Ann. Rev. Nuclear Sci. 7, 330 (1957).

41. Frank, Gammel, and Watson, Phys. Rev. 101, 891 (1956).

42. J. R. Fulco, Phys. Rev. 114, 374 (1959).

43. We obtain this number by assuming multiplicity varies as $(E/E_0)^{1/2}$. This value happens to agree very well with our results, but our statistics do not warrant any conclusions about change in pion multiplicity vs total energy available.

44. R. Gatto, Nuovo cimento 3, 468 (1956).

45. Crawford, Cresti, Douglass, Good, Kalbfleisch, Stevenson, and Ticho, Phys. Rev. Lett. 2, 266 (1959).

FIGURE LEGENDS

Fig. 1.   Arrangement of apparatus to deliver antiprotons to the 30-in. propane

bubble chamber.   Brief descriptions are given in Table I.   This apparatus

was also used for the exposure of several emulsion stacks.

Fig. 2.   The distribution in range of 1069 protons delivered to the bubble

chamber through the same magnetic channel as the antiprotons.

Fig. 3. $\bar{p}$-p Cross sections.   A comparision of theoretical (Ball-Chew model)

and experimental $\bar{p}$-p elastic and annihilation cross sections.   The

experimental points are averages over two energy intervals, 75 to

137.5 Mev, and 137.5 to 200 Mev.

Fig. 4.   Angular distribution for $\bar{p}$-p elastic scattering.   Thirty-one events in

145 meters of antiproton track over an energy range from 75 Mev to 200

Mev are plotted.   The cutoff angle is 25 deg (c. m.)   The theoretical

curve at 140 Mev by Fulco, based on the Ball-Chew model, is shown

for comparison.   Fulco predicts σ_{el} (25 deg) = 58 mb; our results are

47 ± 8 mb.

Fig. 5. $\bar{p}$-C cross sections.   The experimental points are averages over two

energy intervals, 75 to 137.5 Mev, and 137.5 to 200 Mev.   The

theoretical points are obtained by the use of Ball-Chew nucleon-

antinucleon interaction in an optical-model calculation by Bjorklund

and Fernbach.   The theoretical values labeled nonelastic include

charge-exchange and inelastic scattering as well as annihilation.
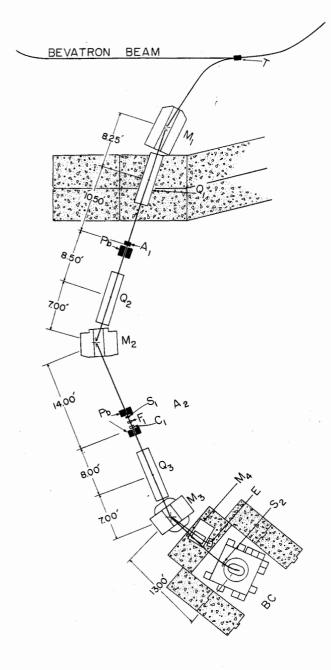
Coulomb effects on elastic scattering are unimportant in the ex-

perimental points and are excluded in the theoretical points.

Fig. 6. $\bar{p}$-C differential scattering. This is a histogram showing our $\bar{p}$-C

elastic-scattering differential cross section including all events of

antiproton kinetic energy between 75 and 200 Mev. An optical-model curve

due to Bjorklund and Fernbach, using the method of Watson and

Riesenfeld and the Ball-Chew phase shifts for 140 Mev, is also

shown.

Fig. 7. Kinetic-energy spectra of the charged pions from hydrogen annihilations.

Only pions with at least 10 cm of track (unless stopping) and which make

an angle of $\geq$ 60 deg with the magnetic field are included.

(a) π^- spectrum, (b) π^+ spectrum.

Fig. 8. Energy histogram of 29 π^0-decay γ conversions observed in hydrogen

annihilations. Each photon has been weighted according to its conversion

probability. Because of the effect of the weighting factor, each unit

of the ordinate represents 50 photons.

Fig. 9. Kinetic-energy spectra of charged pions from carbon annihilations.

Only pions with at least 10 cm of track (unless stopping) and which

make an angle of $\geq$ 60° with the magnetic field are included.

(a) π^- spectrum for in-flight carbon stars, (b) π^+ spectrum for

in-flight carbon stars, (c) π^- spectrum for at-rest carbon stars,

and (d) π^+ spectrum for at-rest carbon stars.

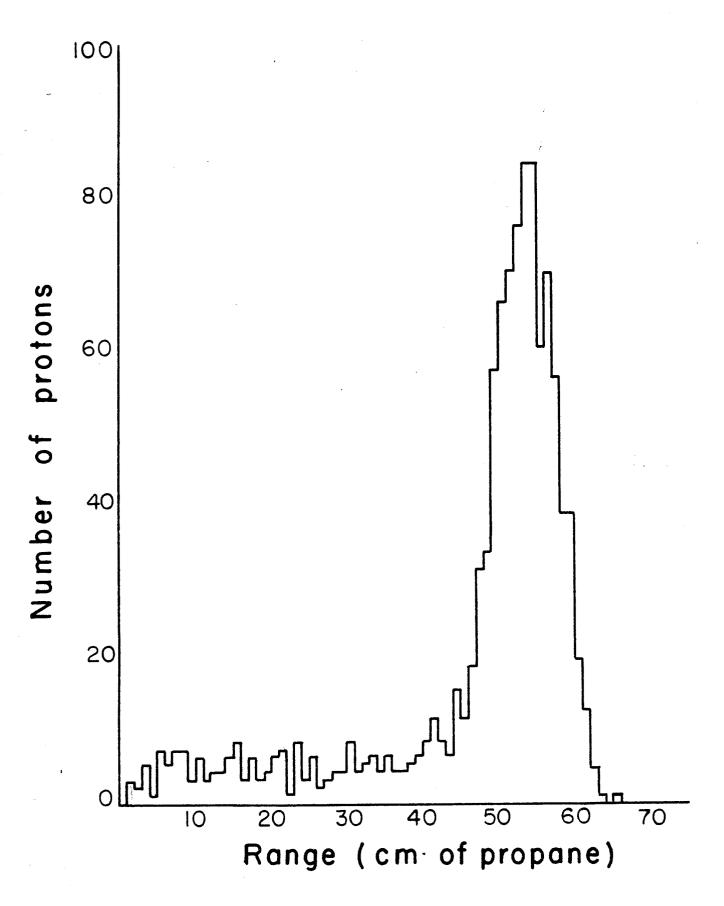Fig. 10. Kinetic-energy spectra of black prongs (all assumed to be protons)

from carbon annihilations (a) in flight and (b) at rest. Only

particles with at least 10 cm of track(unless stopping) and which make an

angle of $\geq$ 60 deg with the magnetic field are included.

Fig. 11. Energy histograms of (a) 23 π^0-decay γ conversions observed in

in-flight carbon annihilations and (b) 25 γ conversions observed in at-

rest carbon annihilations. Each photon has been weighted according to its

conversion probability. Because of the effect of the weighting factor, each

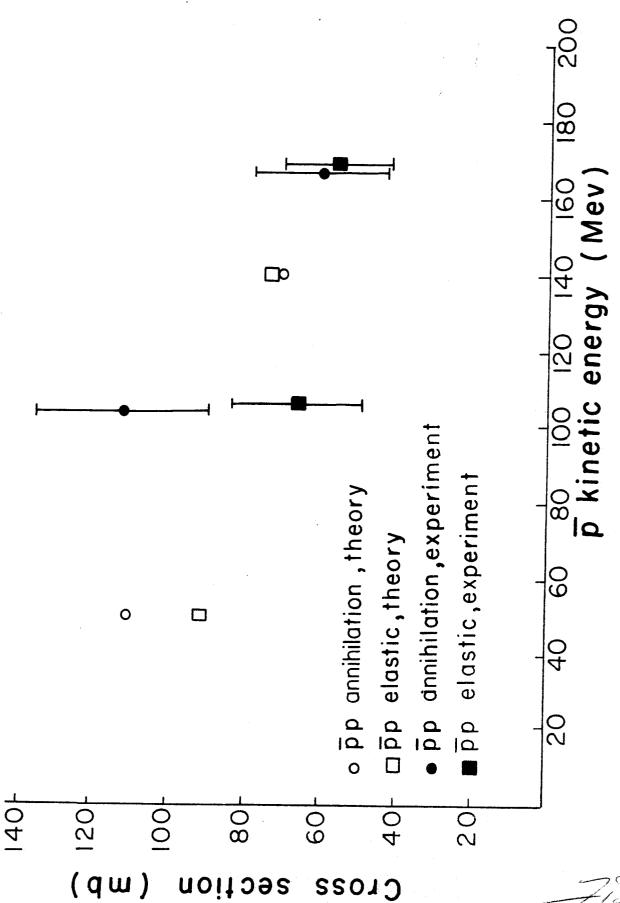unit on the ordinate represents 50 photons.

Fig. 12. Frequency distribution of carbon annihilations according to the total number of charged prongs observed for (a) in-flight carbon stars and (b) at-rest carbon stars.

Fig. 13. Frequency distribution of carbon annihilations according to the total number of charged pions observed for (a) in-flight carbon stars and (b) at-rest carbon stars. Black prongs were ignored in constructing this histogram.

Fig. 14. An antiproton enters at top left of picture and makes a heavy track until it annihilates into three charged prongs near center of picture. Directly below the annihilation is a $K^0 \rightarrow \pi^+ + \pi^-$ event. Above and to the right of the annihilation is a Λ^0 with a projected opening angle near 0°. Event number 28004.

Fig. 15. An antiproton enters at top left of picture and makes a heavy track until it annihilates near center of picture. The longer of the two prongs on the right may be seen to decay, sending a minimum-ionizing particle down and out of the bottom of the picture. This is a $K^+ \rightarrow \pi^+ + \pi^0$ at rest. Event number 36046.

Fig. 16. A kinetic-energy histogram of K particles observed in association with antiproton annihilations. This plot is not corrected for charged-K scanning inefficiency, which is expected to be 100% below 100 Mev and probably decreases with increasing energy.
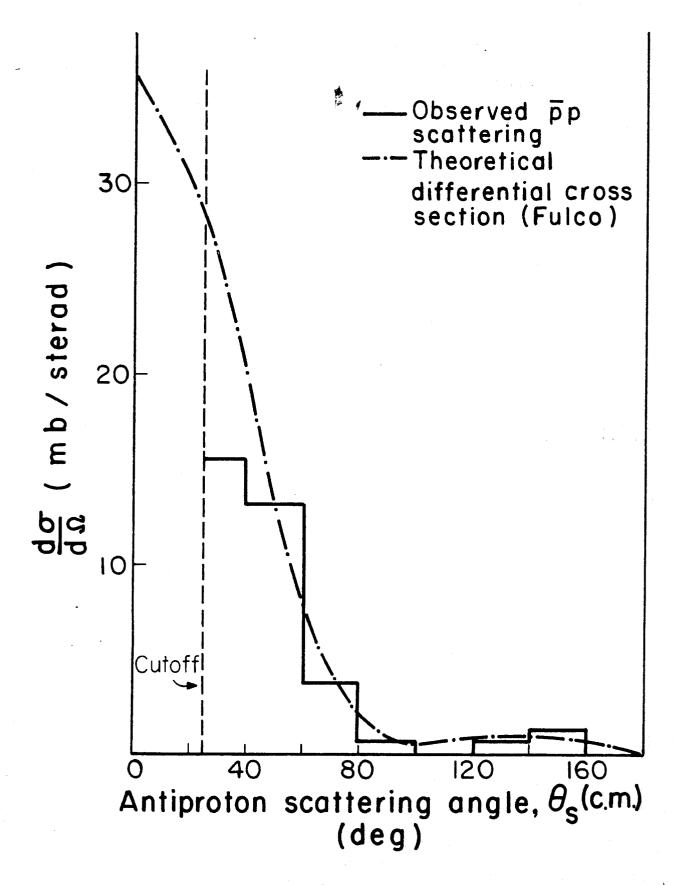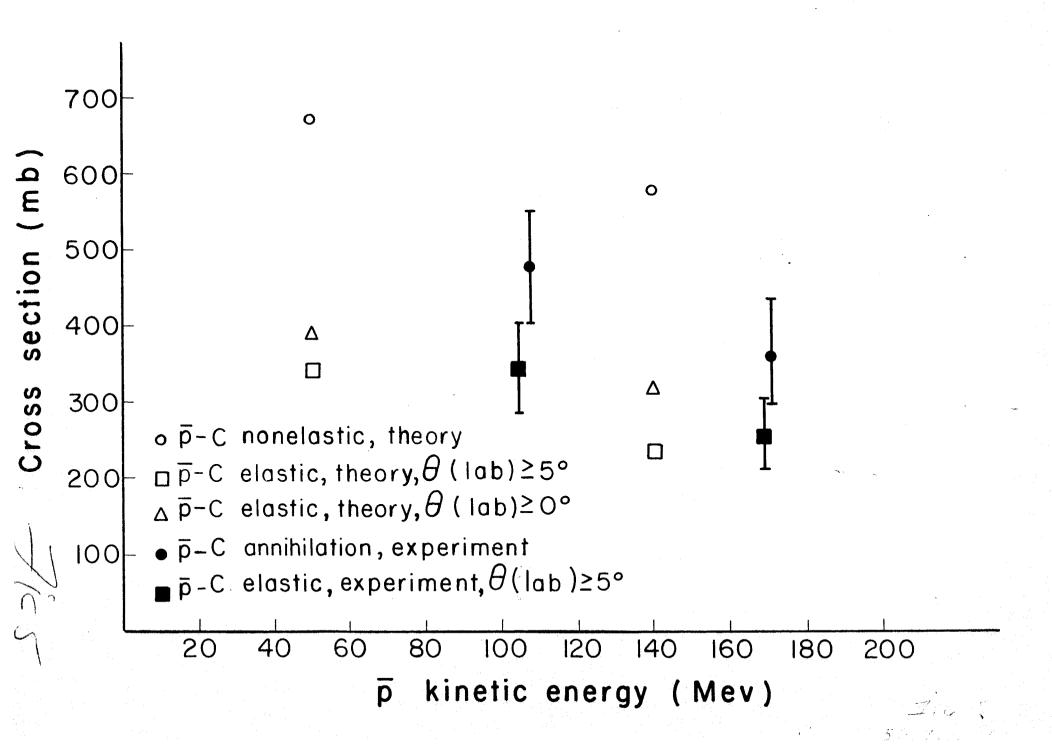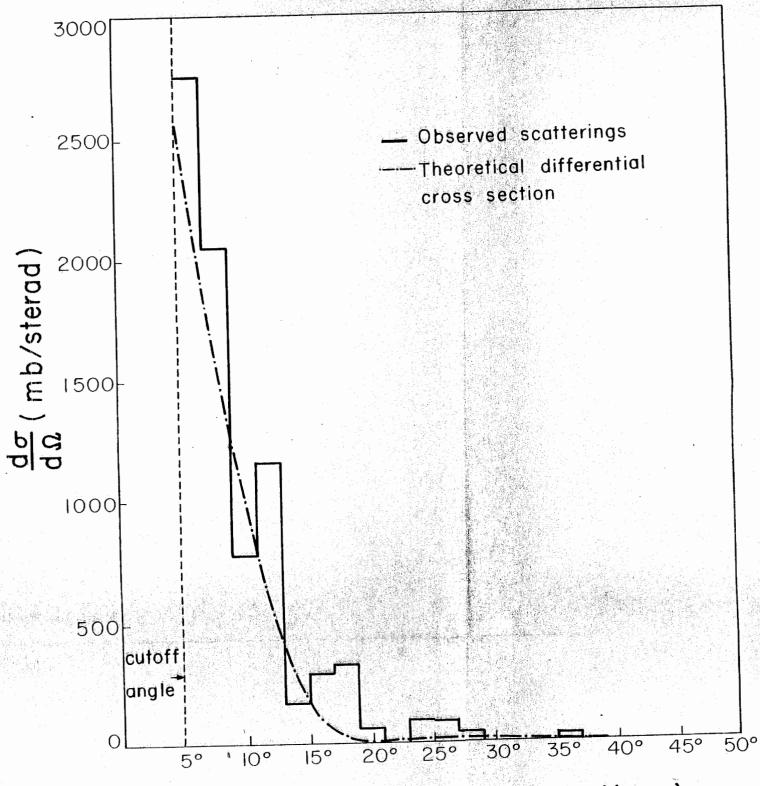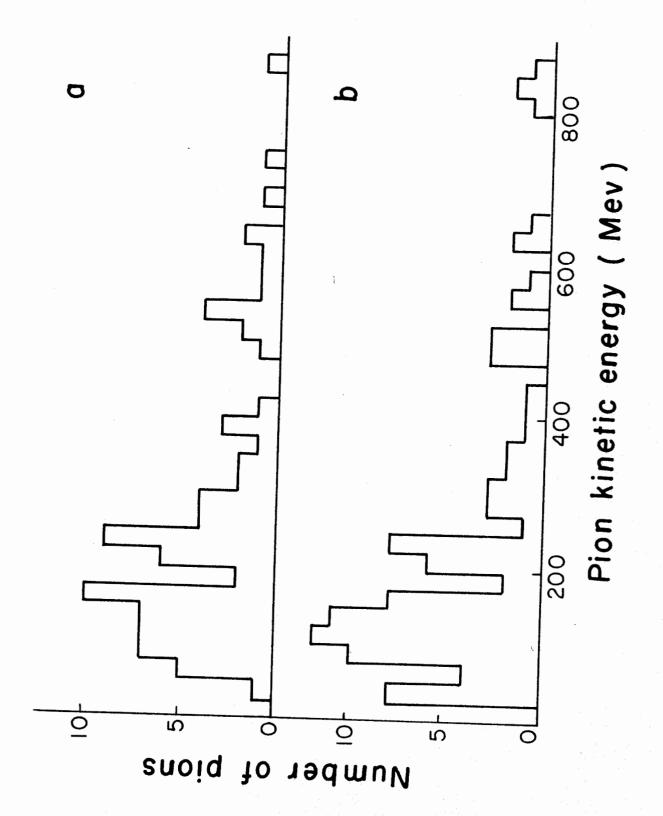
BEVATRON BEAM

T

M_1

8.25'

Q_1

10.50'

P_b A_1

8.50'

7.00'

Q_2

M_2

14.00'

P_b S_1 A_2

F_1 C_1

8.00'

Q_3

M_3 M_4 E S_2

7.00'

13.00'

BC

Fig. 2

Fig 3

The figure is a scatter plot with "Cross section (mb)" on the vertical axis (ranging from 20 to 140) and "p̄ kinetic energy (Mev)" on the horizontal axis (ranging from 20 to 200). The legend shows:
- ○ p̄p annihilation, theory
- □ p̄p elastic, theory
- ● p̄p annihilation, experiment
- ■ p̄p elastic, experiment

Fig 4

Legend:

○ $\bar{p}$-C nonelastic, theory

□ $\bar{p}$-C elastic, theory, θ (lab) $\geq 5°$

△ $\bar{p}$-C elastic, theory, θ (lab) $\geq 0°$

● $\bar{p}$-C annihilation, experiment

■ $\bar{p}$-C elastic, experiment, θ (lab) $\geq 5°$

Cross section (mb) vs. $\bar{p}$ kinetic energy (Mev)

Scattering angle, θ (lab)(deg)

Figure with axes: "Pion kinetic energy (Mev)" (horizontal axis, marked at 200, 400, 600, 800) and "Number of pions" (vertical axis). Two histograms labeled a and b.

Photon energy (Mev)

Relative number of photons

800   600   400   200

3.0   2.0   1.0   0

Fig 8

Pion kinetic energy (Mev)

Cutoff

a

b

420 Mev

Number of protons

Number of protons

Proton kinetic energy (Mev)

Fig. 11

a

Number of annihilations

Total number of charged prongs

b

Number of annihilations

Total number of charged prongs

FIG 13

Fig 14

Legend:
— Identified k's
--- Possible k's

X-axis: K-meson kinetic energy (Mev)
Y-axis: Number of K mesons